General Disclaimer

One or more of the Following Statements may affect this Document

- This document has been reproduced from the best copy furnished by the organizational source. It is being released in the interest of making available as much information as possible.

- This document may contain data, which exceeds the sheet parameters. It was furnished in this condition by the organizational source and is the best copy available.

- This document may contain tone-on-tone or color graphs, charts and/or pictures, which have been reproduced in black and white.

- This document is paginated as submitted by the original source.

- Portions of this document are not fully legible due to the historical nature of some of the material. However, it is the best reproduction available from the original submission.

A STUDY OF HIGH PERFORMANCE ANTENNA SYSTEMS FOR DEEP SPACE COMMUNICATION

The Ohio State University

ElectroScience Laboratory

Department of Electrical Engineering
Columbus, Ohio 43212

STATUS REPORT 2902-2

December 15, 1969 to July 15, 1970

August 1970

Grant Number NGL 36-008-138

National Aeronautics and Space Administration
Electronics Research Center
Cambridge, Mass. 02139

07

REPORT 2902-2

REPORT
by
THE OHIO STATE UNIVERSITY ELECTROSCIENCE LABORATORY
COLUMBUS, OHIO 43212

Sponsor	National Aeronautics and Space Administration Electronics Research Center Cambridge, Mass. 02139
Grant No.	NGL 36-008-138
Research Title	High Performance Antenna Systems for Space Communication
Subject of Report	A Study of High Performance Antenna Systems for Deep Space Communication
Submitted by	ElectroScience Laboratory Department of Electrical Engineering
Date	August 1970

CONTENTS

A STUDY OF HIGH PERFORMANCE ANTENNA SYSTEMS FOR SPACE COMMUNICATION

I. INTRODUCTION

The objective of this program is to study the most recently defined parameters for a high data rate of communication system which can operate between an earth station and a vehicle in space over great distances. An effort will be made to describe and delineate the characteristics of radiating subsystems and their internal sub-divisions which can satisfy the requisite performance criteria for an S-band system. Considerations will be given to the advance technology concerned with the ground based antenna, and where pertinent, to the spacecraft antenna as well. An effort will be made to determine the feasible design approaches for the ground antennas and its component parts. Appropriate design criteria will be investigated analytically, and where possible a comparison will be made with empirically determined results in an effort to define areas of research and development which need long term attention.

The ground-based antennas are discussed in this program as components of a link designed to fulfill the specific function of providing uninterrupted communication from a spacecraft to the earth at planetary distances. For obvious reasons, the most attention is given the down link aspects using a carrier frequency of 2.3 GHz, since a frequency in this region has advantages for an all-weather ground station and is presently in use in the NASA Deep Space Instrumentation Facility. It is assumed also that future mission plans will require information rates of the order of 10^4 to 10^7 bits/second with a given probability of error, 10^{-2} to 10^{-5}. These parameters imply a specific system performance in terms of bandwidth and signal-to-noise ratio. When the characteristics of the available transmitter and receiver are evaluated or assumed, the required performance characteristics of the overall radiating system are determined either directly or by implication. The overall radiating system is taken to include the combination of the spacecraft and the ground or relay station antenna equipment in their inevitable environment. Thus, for this study, certain gain and aperture requirements will be assumed nominal as parameters to satisfy a variety of space missions.

There are two general areas of concern that must be investigated relative to the ground-based receiving system which of necessity must be large compared to wavelength to achieve the desired performance characteristics. The first involves questions about the received signal to noise level or the gain that must be provided to handle it. Considerations must be given to methods by which it may be enhanced, and the limitations that may be encountered during the various phases of a mission. The second area embraces questions about the contributions made to the noise of the communications link, the manner in which these are introduced, and methods by which they may be minimized. These questions are, of course,

interrelated, and the limitations encountered are intensely practical and economic, as well as theoretical. For this study, emphasis will be given to the first area and when necessary, results of other investigations into the questions involved in the second area will be used.

The requirement of a minimum signal to noise level forces the sum of the gains of the space and ground antennas to be of some value that can be specifically determined for a particular mission. It is important to be able to allocate the antenna gains at each end of the link according to reasonable expectations concerning the practical designs and performance characteristics that can be accomplished in the next ten to fifteen years. An optimum allocation of these gains is difficult although some progress has been made along these lines. For this study nominal values are used as parameters in an effort to establish quantitative relationships between pertinent dimensions and techniques. It has been shown that at 2.3 GHz, the sum of the antenna gains on future missions can be estimated to be about 110 dB to achieve a data rate of 10^6 bits/second. This is about a 20 dB increase over the gains specified for the 1971 Vogager Mission at 1 AU as a basis for comparison. If the spacecraft antenna is postulated to be capable of 30-40 dB of gain using a transmitter with 50-100 watts of power, then the ground based receiving system must be studied for the following range of parameters:

Antenna Gain -- 60 to 80 dB
Data Rate -- 10^4 to 10^7 bits/second
Error Probability -- 10^{-2} to 10^{-5}

Final results will be given for this entire range of parameters although nominal values will be used to illustrate and expedite the discussion of various techniques during the intermediate phase of this program.

Because of the significance of the noise level in determining the overall gain requirement, many studies have been directed to a consideration of the noise that competes with the signal and is collected and introduced at the ground end of the down link. The convention of treating the noise as resulting from an equivalent antenna temperature has been followed in this program. Since the noise level is highest when the antenna beam is directed at or near a noise source, attention is being paid to techniques which can be used to mitigate these deleterious effects in certain special mission circumstances.

The characteristics of high gain techniques, either electrical or mechanical, form essential parts of tradeoffs in system accuracy, reliability, and cost. Of course practical compromises must be made for certain aspects of a particular mission. These compromises will depend on the techniques available for directing or steering the receiving beam on the ground as compared with those for controlling the vehicle attitude. Three types of steering mechanisms are possible for spacecraft antenna systems: mechanical (as for large appendage antennas); electromechanical; and electronic or inertialess. Electronic techniques offer the greatest versatility with regard to

communications between a vehicle in space and earth. These are two generic types: those that require external controls to phase the elements properly and those that are self-steering. The externally controlled systems, such as the conventional phase array, need an external sensor (IR, RF, or ground station) to point the beam, and a computer, a phasing network, and an attitude sensing device to point the beam appropriately. In the self-steering system, however, attitude information is presented to the antenna system by a pilot beam from a ground station, and electronic circuitry senses the phase of incoming pilot signals to position a beam in the direction of these pilot signals. Multiple beam systems may be accommodated by the use of diplexers and multiple electronic channels. Each of these spacecraft systems is being worked on by various research and development groups throughout the country and abroad. Appropriate results of these efforts will be used to achieve stated objectives of this program.

II. PROGRAM DESCRIPTION

As it has been discussed in earlier reports on this program, there are basically two fundamental kinds of antenna systems that can be used in applications requiring large apertures. The first is a large mechanically steerable paraboloidal reflector or a number of smaller reflectors of this type which are connected and fed as an array and mechanically steered as individual radiators. The second is a phased array with stationary or fixed apertures composed of subapertures whose relative phasing controls the direction of the antenna beam. Thus, this program considers the various aspects and organizations of the following generic types of large ground based antenna systems:

A. A SINGLE LARGE APERTURE -- mechanically steerable.

A system of this type will be discussed in this study only to provide a basis for the comparison of performance characteristics with the other systems listed below. Technical descriptions and data appropriate to this portion of the program have been obtained from several organizations not directly involved in this study.

B. AN ARRAY OF LARGE DISHES -- each of which is mechanically steerable.

The appropriate organization of a system of this type is considered herein with respect to the element spacing and their interaction.

C. A PHASED ARRAY OF SMALL CLOSELY SPACED ELEMENTS ORGANIZED INTO SUBAPERTURES -- electronically steerable.

Most of the effort in this program will be concerned with the various organizations, the feeding techniques, and the elements appropriate to this type of system.

D. A SELF-STEERING ARRAY -- rapidly switched multiple beams or adaptive systems.

Systems of this type can be used to mitigate the effects of high intensity noise sources and employed in conjunction with the system of type C to accomplish optimum mission performance. The feasibility of application of these techniques for a high data rate communication system is being investigated during the course of this program.

Consideration is being given to the capabilities and limitations of each of the above types during the course of this study and a report* made in the above listed categories. Although some of the results and information described therein were obtained in one research or industrial institution and some in another, this report, as have previous reports, was written with the idea of integrating the results of various research efforts and techniques in such a way as to implement the objectives of the program without regard to the actual source of the material.

This present program has been active for the past eight months in the ElectroScience Laboratory (ESL) at The Ohio State University. However, it is a natural outgrowth of a cooperative effort between the personnel of the Center for Research in Engineering Science (CRES) at the University of Kansas and ESL, which has been running under Grant Number NGR 17-004-013 for the previous 2 1/2 years. Thus, the entire program has uncovered a number of technical details with regard to the ground based portion of the system and has been able to provide a framework for evaluating various large ground-based antenna systems. Additionally it has uncovered a number of technical details that need further consideration and invention. However, recent efforts on other programs have indicated that information concerning performance characteristics and production costs of low-loss transmission lines, radiating elements, and other systems are now being determined and can be used in the design of any reasonable ground-based system. To provide an optimum overall communications system, there is a need, however, for more effort to determine the behavior of various high performance antennas on spacecraft which are designed for future earth orbital mission operations.

III. ACTIVITIES DURING THE PERIOD

In this period, several aspects of the program description given in Section II were pursued and essentially completed. Primarily, these concerned the efforts on the adaptive array techniques which have been completed and culminated in a report Number RF 2902-1 that represents the doctoral dissertation of Robert L. Riegler. In addition, studies

---

*Status Report IV, Grant Number NGR-17-004-013, CRES - University of Kansas.

involving aperture blockage among arrays of closely spaced large dish antennas which are mechanically scanned have been pursued on both a theoretical and an experimental front. These items are to be summarized briefly in a qualitative manner in this section and reported in detail in the appropriate section of the Technical Summary in Section IV.

1) During this semi-annual period the signal processing equipment for an adaptive array study was completed, tested, and reported as RF 2902-1. The following is an abstract of this report:

Adaptive optimization of signal-to-noise ratio in receiving arrays is presented for both background sky noise and coherent jamming type noise interference.

The array weighting coefficients which maximize SNR are derived for an array subjected to uniform background antenna noise. An array model of half-wavelength dipoles placed over a ground plane is analyzed in detail to show the effects of such factors as mutual coupling.

An adaptive array that rejects undesired or interfering signals is presented. The array pattern is controlled by an adaptive feedback system based on a steepest-descent minimization of mean square error. Here error is defined as the difference between the array output and a locally generated reference signal. Minimization of mean square error is closely related to maximization of signal-to-noise ratio.

A two-element S-band adaptive array has been built, and its experimental performance is discussed. Typical antenna patterns for various desired and interfering signals are shown, as well as measured transient response. Finally, some experiments showing the array behavior with modulated signals are described.

The results show that such an antenna system is capable of automatically rejecting interfering signals, subject only to certain basic constraints. No a priori information concerning the angles of arrival of the signals is required. Detailed knowledge of the waveforms of the desired and interfering signals is also not needed, although the spectral density of the desired signal must be known.

2) A continuing effort is being made to determine quantitatively the performance characteristics of an array of independently steerable paraboloids by mechanical means. Consideration is being given to the proper size and separation of large disk antennas to achieve the requisite high performance characteristics over a $\pm 60^\circ$ angle of scan. A minimum separation distance must be determined in order to utilize a given aperture size most efficiently. However, as the separation is decreased, the interference between adjacent paraboloids becomes important, especially at large scan angles. This interference phenomenon is being investigated by several theoretical approaches in an effort to

determine quantitatively the pattern degradation of closely spaced paraboloidal antennas which can be mechanically scanned. As the separation is increased, the formation of grating lobes in a large array of parabolic reflectors presents a problem which requires a detailed study and a quantitative assessment of the results of overall system performance.

The activities on this portion of the program are continuing on both a theoretical and computational basis as well as on an experimental verification approach. The theoretical results in this portion of the program have been completed using the geometrical theory of diffraction (GTD). The employment of the GTD to solve the blockage problem associated with an array of closely spaced paraboloidal antennas turned out to be straight-forward application of a simple technique. If has been used very successfully to predict radiation patterns of various antenna systems, especially antenna systems with reflector surfaces. The computational effort to present these results is in progress and should be completed shortly. There remains, however, some simple experimental activities which are to be completed shortly in an effort to verify the basic theoretical formulation that is to be presented. This work comprises the doctoral dissertation of Mr. Cheng Don, and it is described in detail under Section IV-B. It is expected that the entire effort on aperture blockage will be completed during the summer of 1970 and carefully documented in a separate technical report.

IV. TECHNICAL SUMMARY

The discussion summarizing the technical effort of this report period will be given in a condensed format using the program description described in Section II in an effort to delineate the work accomplished according to the appropriate documentation for this effort.

A. A SINGLE LARGE APERTURE - MECHANICALLY STEERABLE
(See Status Report Number 4, dated 15 February 1970 on Grant Number NGR-17-004-013)

B. AN ARRAY OF LARGE DISH ANTENNAS

1) Introduction

As it has been mentioned before, an array of independently mechanically steerable paraboloids with proper size and separation may be one of several workable approaches capable of achieving the high gain requirement for the DSCS. To provide the requisite scanning angle of $\pm 60^{\circ}$ without interference between adjacent paraboloids, the spacing between reflectors must be kept at a reasonable distance which is larger than the diameter of the paraboloids. Thus, a minimum separation distance must be determined which utilizes a given aperture size most efficiently. As the separation is increased, the formation of grating lobes in a large array of parabolic reflectors constitutes a serious difficulty for which no generally satisfactory solution has yet been developed. The problem can be visualized if the array pattern is considered as the product of an element pattern and an array factor.

The element pattern consists of the radiation pattern produced by a parabolic reflector, while the array factor is the pattern of an array of isotropic radiators which is a two-dimensional grating lobe pattern. The array factor can be steered electronically by shifting the phase between elements while the element pattern is directed by the mechanical movement of the individual dishes. In the ideal case, the element pattern and a single lobe of the array factor will both point in the desired direction. Multiple beams appear, however, when more than one grating lobe falls within the main beam of the element factor; this condition occurs when the array spacing is substantially greater than the diameter of the subapertures.

It can be easily shown that the spacing of the grating lobes from the main beam can be increased by a decrease in the separation of the parabolic reflector antenna elements. However, if this spacing is decreased, the diameter of the reflectors must also be decreased so that the effective scan range can be maintained, while at the same time more array elements must be added to meet the gain requirement. The end result will be a broader element pattern which in turn will ensure that the grating lobes will have essentially the same amplitude relative to the main beam. The beamwidth of both the main beam and the grating lobes will, for all practical purposes, remain the same as long as the overall array dimensions remain unaltered. The fine grain structure around the various lobes will change, however, as more elements are added. Similarly, if the spacing between the elements is increased, and the diameter of the reflectors is increased correspondingly, the grating lobes will be moved in closer to the principal beam. Once again the relative amplitude and beamwidth of all the grating lobes should remain essentially constant.

There are some esoteric techniques available to suppress the size of the grating lobes. A possibility exists that the grating lobes adjacent to the principal beam may be reduced in amplitude by the use of random spacing among the array elements. However, it is anticipated that the selection of such a design will prove to be an extremely difficult problem. Another means of suppressing the grating lobes might involve the use of an auxiliary array that could be steered and phased to cancel out any given lobe. A major difficulty that might be anticipated from such a scheme would be the obtaining of sufficient gain from the auxiliary array.

The juxtaposition of spacing and reflector size discussed above is predicted on little or no interaction between the elements as a function of scan angle. When this interaction effect is taken into account an entirely different solution may be obtained for the competing parameters. Thus, it shall be the purpose of this section to study the problems associated with being able to analytically determine a spacing and antenna size which is optimum between the interference effects at minimum separation, and the grating lobe effects at a maximum distance commensurate with high aperture efficiency. Since the theory and manipulation of the array factor and element pattern is available elsewhere, the effort herein shall be concerned with methods

and techniques for analyzing the interaction effects between large parabolic reflectors in a relatively closely spaced array.

An analysis of the blocking effect of a closely spaced array obtained by the consideration of the geometric optics only has been done in paragraph (2). First, the field in Franhofer region for an antenna system of two closely neighboring paraboloids has been formulated; then the field for a linear array of N-paraboloid is obtained. In these expressions, they show clear evidence of the interaction between neighboring paraboloids due to the close separation between them.

The analysis in Sec. B-2 is based only upon the geometrical ray theory which is a valid high frequency approximation. The first correction factor to this geometrical ray approximation is obtained in Sec. B-3 by applying the geometrical theory of diffraction. The surface current density on a parabolic reflector due to this correction factor has been obtained in addition to the current density due to the geometrical ray contribution.

2) Theoretical consideration of the interaction between neighboring paraboloid antennas: the blocking effect of a closely spaced array

a) Introduction - It has been learned that some mutual coupling measurements on neighboring paraboloid antennas has been done by Andrews (Ref. B-1) for Collins Radio Co. and a similar measurement also has been done recently by Reiche (Ref. B-2) at the Hughes Aircraft Co. It seems, however, that there is no literature concerning theoretical analysis available. Therefore, it is desirable to develop the analytical form which governs the fields of a paraboloid antenna as a function of scan angle in the presence of neighboring array elements of an identical kind.

The far field transmitting and receiving patterns of the neighboring paraboloidal antennas with their vertices far apart will be the vector sum of individual contributions at the field point and the vector sum of the receiving fields at individual feeds respectively. In fact, the transmitting and receiving patterns of the paraboloidal antennas system in Fraunhofer region are the same in this case. As the positions of the vertices of the paraboloidal antennas get near enough, the interaction between them can no longer be negligible. The interaction between the paraboloidal antennas for which the system being used for transmitting function and that for which the system being used for receiving function will constitute different problems. However, the final analysis for both transmitting and receiving functions of the system will lead to the same result. Thus the transmitting and receiving modes of the system merit no separate investigation. In this report, the following paragraphs are devoted to the transmitting mode of an array of paraboloidal antennas.

The elements used in the array are parabolic reflector antennas. The reflector is assumed to have a perfectly conducting surface and is illuminated by a primary feed antenna located at its focal point. The aperture of the reflector is assumed to have a tapered illumination.

The fields in the far-zone region of a two-element array are obtained both with and without blockage in Sec. B-2c. The field in the far-zone region of a linear array of N identical parabolic reflectors is formulated in Sec. B-2d. A simple case in which the array pointing direction is (θ',ϕ') and the observation point locates at $P(R,\theta,\phi)$ with $\phi' = \phi = \pi/2$ is studied in Sec. B-2e. The angles (θ',ϕ') and (θ,ϕ) are defined in Sec. B-2b and Sec. B-2c respectively.

(b) Consideration of the Coordinate Systems - The fixed coordinate system (x,y,z) with origin at point 0 will be used to define the observation point in space. The paraboloid coordinate system (x',y',z') with origins at the vertex of each paraboloid will be used to define the source points in space. The condition of the paraboloid coordinate system is specified in such a way that when the axis of the paraboloid (z'-axis) points in its zenith direction (in the direction of z-axis) the remaining x' and y' axes coincide with the fixed x and y axes respectively. That is, when paraboloid is at its zenith direction, the coordinates x', y' and z' coincide with the fixed coordinates x, y and z respectively. In order to define uniquely the pointing direction of the paraboloid in the direction (θ',ϕ') in the fixed coordinate, the axes of the paraboloid are being rotated as follows: first, x'-axis is rotated by an angle ϕ' in azimuth direction with z-axis as the axis of rotation. Hence, the angle between axes y' and y is ϕ'. Next, z'-axis is rotated by an angle θ' with y'-axis as the axis of rotation. Thus, the angle between axes z' and z is θ' and the angle between x-axis and the projection of x'-axis on the xy plane is ϕ'.

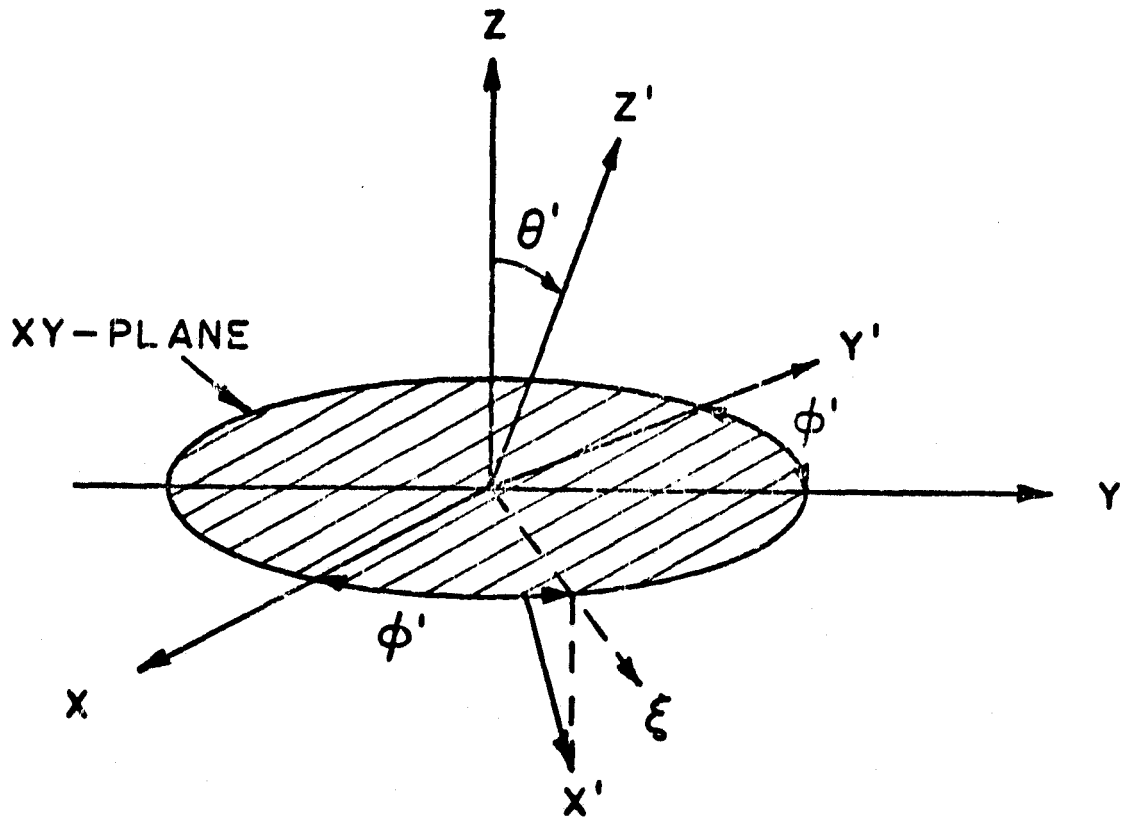

Let the direction of the projection of x'-axis on the xy plane be ξ, then

$$\bar{a}_y, \bar{a}_{y'} = \phi'$$

$$\bar{a}_x, \bar{a}_\xi = \phi'$$

$$\bar{a}_z, \bar{a}_{z'} = \theta'$$

$$\bar{a}_{x'}, \bar{a}_\xi = \theta'$$

By these two rotations, the paraboloid coordinates have been uniquely defined in the fixed coordinate system. Hence,

(B-1)

$$\bar{a}_{x'} = \bar{a}_x \cos\theta' \cos\phi' + \bar{a}_y \cos\theta' \sin\phi' + \bar{a}_z(-\sin\theta')$$

$$\bar{a}_{y'} = \bar{a}_x (-\sin\phi') + \bar{a}_y \cos\phi' + \bar{a}_z\, 0$$

$$\bar{a}_{z'} = \bar{a}_x \sin\theta' \cos\phi' + \bar{a}_y \sin\theta' \sin\phi' + \bar{a}_z \cos\theta'$$

(c) Fields in Fraunhofer Region for an Antenna System of Two Neighboring Paraboloids

A two-element array of identical parabolic reflector antennas with their axes pointing in the direction (θ',ϕ') is shown in Fig. B-1. The first parabolic reflector is located with its vertex at the origin O of the fixed rectangular coordinate (x,y,z). The second parabolic reflector is located with its vertex at point A along the y-axis a distance "d" away from the origin. The aperture radius and the focal length of the parabolic reflectors are denoted by "a" and "f" respectively. The unit vectors $\hat{a}_{v1}$, $\hat{a}_{v2}$, and $\hat{a}_R$ are in the direction of v_1, v_2, and R respectively. The distance from the vertex to its aperture for a parabolic reflector is denoted by z_o which can be found to be $a^2/4f$.

Let the field distribution over the circular aperture by designated by

(B-2) $$F(\rho,\psi) = A(\rho,\psi)\, e^{jk\Psi(\rho,\psi)}$$

with amplitude distribution $A(\rho,\psi)$ and phase distribution $\Psi(\rho,\psi)$; where ρ and ψ are the variables for the polar coordinates on the aperture.

For the far-zone region, the field due to a single aperture is given by

(B-3)

$$U_p = \frac{j}{2\lambda} \frac{e^{-jkR}}{R} (1 + \gamma) e^{jkz_o\gamma} \cdot \int_{\psi=0}^{2\pi} \int_{\rho=0}^{a} F(\rho,\psi) e^{jk\rho[\alpha \cos \psi + \beta \sin \psi]} \rho d\rho \, d\psi$$

where

(B-4) $$z_o = \frac{a^2}{4f}$$

$$\gamma = \sin\theta \sin\theta' \cos(\phi-\phi') + \cos\theta \cos\theta'$$

$$\alpha = \sin\theta \cos\theta' \cos(\phi-\phi') - \cos\theta \sin\theta'$$

$$\beta = \sin\theta \sin(\phi-\phi')$$

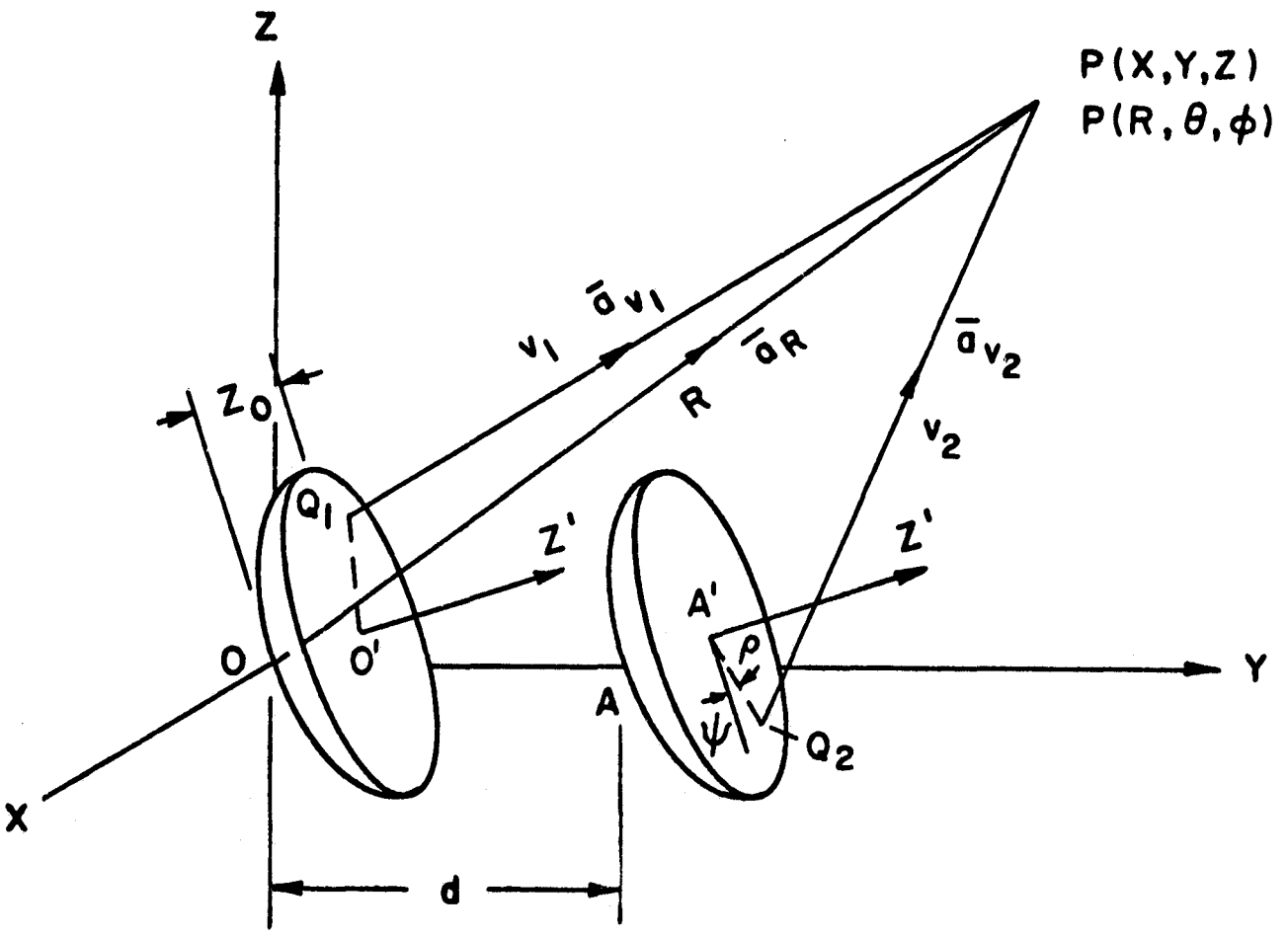

Fig. B-1.

For the configuration in Fig. B-1, the total field at observation point due to the identical aperture distribution $F(\rho,\psi)$ on apertures No. 1 and No. 2 is

(B-5)

$$U_p = U_{p_1} + U_{p_2}$$

$$= \frac{j}{2\lambda} \frac{e^{-jkR}}{R} (1+\gamma) e^{jkz_o\gamma}$$

$$\cdot \int_0^{2\pi} \int_0^{a} F(\rho,\psi) e^{jk\rho[\alpha \cos \psi + \beta \sin \psi]} \rho d\rho \, d\psi$$

$$+ \frac{j}{2\lambda} \frac{e^{-jkR}}{R} (1+\gamma) e^{jkz_o\gamma} e^{jkd \sin \theta \sin \phi}$$

$$\cdot \int_0^{2\pi} \int_0^{a} F(\rho,\psi) e^{jk\rho[\alpha \cos \psi + \beta \sin \psi]} \rho d\rho \, d\psi$$

Equation (B-5) is the total field at observation point without considering the blocking effect. In the case that the separation between the neighboring paraboloids is not large enough, the blocking effect due to the geometric optics obstacles has to be taken into account when the system scans away from its zenith direction. In the latter case, the first aperture of the paraboloid with vertex at origin is partially blocked by the presence of the second paraboloid with vertex at A in Fig. B-1.

If it is assumed that the beam diameter equals the element aperture diameter, the separation between two adjacent elements required for no blockage is given by

(B-6) $$d = \frac{2a}{\cos \theta_m}$$

where

d = separation between elements (parabolic antennas)
a = radius of element apertures
θ_m = maximum polar angle coverage for which no aperture blockage occurs when scanning.

Theoretically, for an angle coverage up to 90 degrees, the separation d has to be infinity in order to have no blockage. The normalized minimal separation with respect to the diameter of element apertures vs the maximum polar angle coverage is shown in Fig. B-2. It is seen that for an

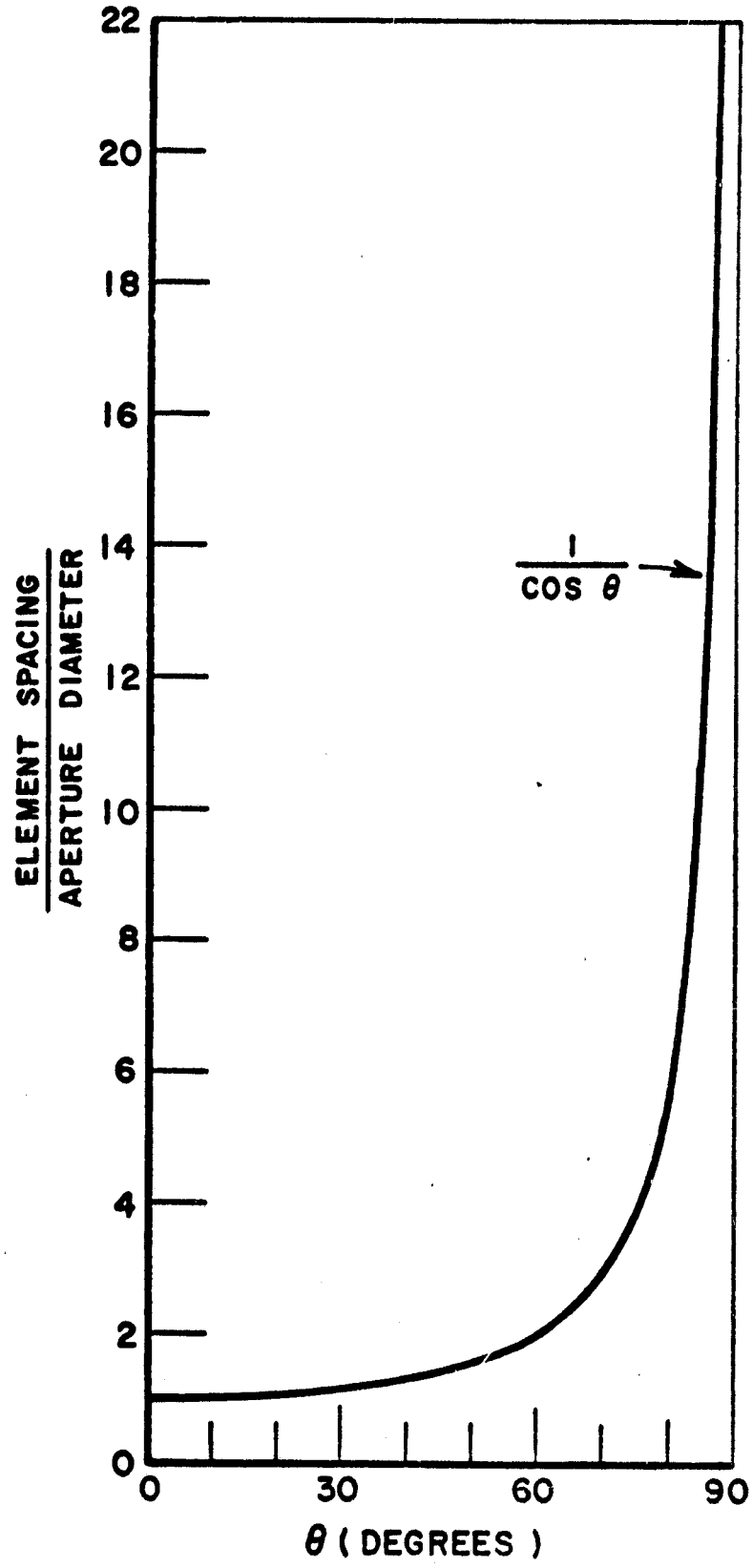
ELEMENT SPACING / APERTURE DIAMETER
22
20
18
16
14
12
10
8
6
4
2
0
1 / cos θ
0
30
60
90
θ (DEGREES)

Fig. B-2.

aperture diameter of 30 ft with maximum angle coverage θ_m of 60 degrees, the minimal separation required for no blockage is 60 ft (twice the size of the aperture); however, for θ_m of 87 degrees (i.e., for an elevation angle of 3 degrees above horizon), the separation increases up to approximately 600 ft (20 times the size of the aperture).

On the other hand, with a given aperture radius "a", the blockage will not occur until the array pointing direction θ' reaches certain value for a given element separation d = pa in terms of the aperture radius by a constant p. Let this "certain value" of array direction θ' for a given d = pa be θ_b'. Then θ_b' can be obtained as

$$\theta_b' = \cos^{-1}\left(\frac{2a}{d}\right) = \cos^{-1}\left(\frac{2}{p}\right) \tag{B-7}$$

For the scan angles less than or equal to θ_b', there exists no blockage in a geometrical optics sense; for scan angles larger than θ_b', blockage occurs. The dependence of θ_b' on the element separation d is shown in Fig. B-3.

Considering the blocking effect due to the geometrical optics obstacles, the field in far-zone region can be taken care of as follows: looking back along z'-axis toward the vertices, the overlap portion of the adjacent apertures due to scanning away from its zenith direction is shown in Fig. B-4. The distance d' can be found as

$$d' = d\sqrt{1 - \sin^2\theta' \sin^2\phi'} \tag{B-8}$$

and

$$d_\ell = 2a - d' = 2a - d\sqrt{1 - \sin^2\theta' \sin^2\phi'} \tag{B-9}$$

where d' is the distance between the axes, which is the projection of the separation d of the vertices of the paraboloids on the plane perpendicular to z'-axis, when the axes point at (θ',ϕ') direction and d_ℓ is the overlap distance along this projection. It is noted that if d^ℓ is larger than or equal to the aperture diameter, there is no blockage. The blockage occurs when the corresponding d' for an arbitrary array pointing direction (θ',ϕ') is less than the aperture diameter. For the latter case, the overlap angle Ω is given by

$$\Omega = \cos^{-1}\left(1 - \frac{d_\ell}{2a}\right) \tag{B-10}$$

The blocked area A_b which is the shaded area in Fig. B-4 can be found as

$$A_b = 2\left[a^2\Omega - \left(a - \frac{d_\ell}{2}\right) \; a \sin\Omega\right] \tag{B-11}$$

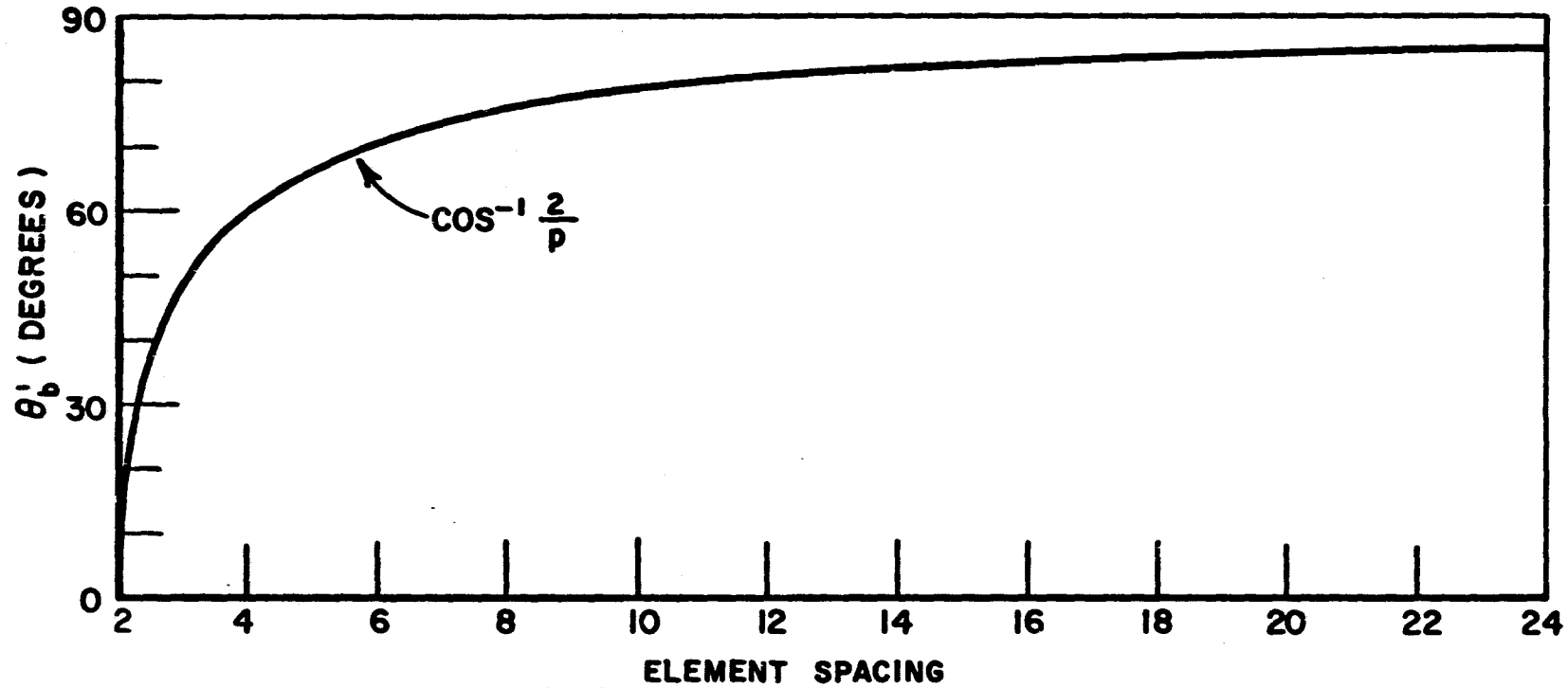

$$p = \frac{\text{ELEMENT SPACING}}{\text{RADIUS OF APERTURE}}$$

Fig. B-3.

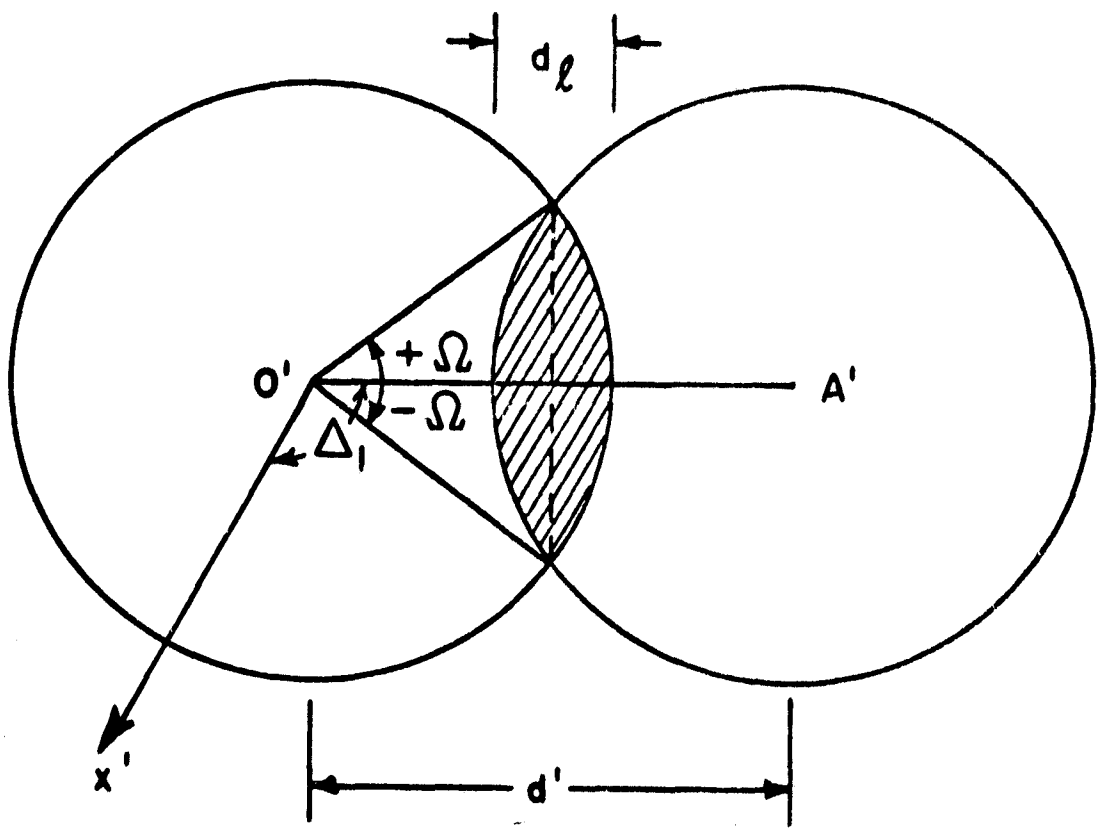

Fig. B-4.

The blocking effect can be taken care of by subtracting the part of contribution due to the blocked aperture; thus

$$(B\text{-}12) \qquad U_{p1} = \frac{j}{2\lambda} \frac{e^{-jkR}}{R} (1+\gamma)\, e^{jkz_o\gamma} [I - I_b]$$

with

$$(B\text{-}13) \qquad I = \int_0^{2\pi} \int_0^{a} F(\rho,\psi) e^{jk\rho[\alpha \cos \psi + \beta \sin \psi]}\, \rho d\rho\, d\psi$$

$$(B\text{-}14) \qquad I_b = \int_{\Delta_1-\Omega}^{\Delta_1+\Omega} \int_{\rho(\psi)}^{a} F(t,\psi) e^{jkt[\alpha \cos \psi + \beta \sin \psi]}\, t\, dt\, d\psi$$

where I is the contribution from the whole aperture and I_b is the contribution from the blocked part of the aperture. The parameter Δ_1 is the angle between the unit vector of the projection of $\hat{y}$ onto the x'y'-plane of the blocked aperture and the unit vector $\hat{x}'$; it is found to be

$$(B\text{-}15) \qquad \Delta_1 = \tan^{-1} \frac{\cos \phi'}{\cos \theta' \sin \phi'}$$

The lower limit of integration, $\rho(\psi)$, is governed by

$$(B\text{-}16) \qquad a^2 = \rho^2 + d'^2 - 2\rho d' \cos(\psi - \Delta_1)$$

One of the two possible roots has to be properly chosen for different ranges of the pointing angle θ' as it will be shown in Sec. B-2d. Therefore, the total field at observation point due to both apertures with blockage becomes

(B-17)

$$\begin{aligned} U_p &= U_{p1} \text{ (partially blocked)} + U_{p2} \text{ (unblocked)} \\ &= \frac{j}{2\lambda} \frac{e^{-jkR}}{R} (1+\gamma)\, e^{jkz_o\gamma} \cdot [I - I_b] \\ &\quad + \frac{j}{2\lambda} \frac{e^{-jkR}}{R} (1+\gamma)\, e^{jkz_o\gamma} \cdot I \end{aligned}$$

where I and I_b are given in Eqs. (B-13) and (B-14).

(d) Fields In Fraunhofer Region for a Linear Array of N-Paraboloids

The array is composed of N identical paraboloids and it is assumed that they point in the same direction simultaneously without delay.

The total blocked area A_b for a linear array of N identical paraboloidal antennas is the sum of the first (N-1) blocked area for the system of two-element array given in Equation (B-11). Hence, A_b becomes

$$(B\text{-}18) \qquad A_b = (N-1) \cdot 2a^2 \left[\Omega - \frac{p}{2} \cos\theta' \left(1 - \frac{p^2}{4} \cos^2\theta' \right)^{1/2} \right]$$

The total aperture A of an array of N-element with no blockage is given by

$$(B\text{-}19) \qquad A = N(\pi a^2)$$

The total effective aperture A_u of an array of N-element with blockage thus becomes

$$(B\text{-}20) \qquad A_u = a^2 \left\{ N\pi - 2\left[\Omega - \frac{p}{2} \cos\theta' \left(1 - \frac{p^2}{4} \cos^2\theta' \right)^{1/2} \right] \right\}$$

where

N = number of elements in an array
a = radius of individual aperture
Ω = angle of overlap defined in Equation (B-10)

p = a constant defined by the relationship given as d = pa, where d is the separation between adjacent elements
θ' = angle of scan or the pointing direction of an array.

It is desirable to know the percentages of the blocked and the effective apertures over the total aperture A with no blockage. Let r_b and r_u be the ratios of A_b/A and A_u/A respectively, then they are given as

$$(B\text{-}21) \qquad r_b = \frac{N-1}{N} \cdot \frac{2}{\pi}\left[\Omega - \frac{p}{2}\cos\theta'\left(1 - \frac{p^2}{4}\cos^2\theta'\right)^{1/2}\right]$$

$$(B\text{-}22) \qquad r_u = 1 - r_b$$

It is noted that the ratio r_b and r_u are functions of parameters N, p (or d, the element separation), and the array pointing direction θ'. They are independent of the aperture size. It is also noted that the above expressions are valid for an aperture distribution of uniform amplitude and phase.

The ratios r_b and r_u vs the element separation for a given array direction θ' have the same significance of the curve θ_b' vs the element separation as given in Fig. B-3. It has shown that for the scan angles less than or equal to the corresponding angle θ_b' given in Equation (B-7), there exists no blockage, $r_b = 0$ and $r_u = 1$. For the scan angle larger than θ_b', the blockage occurs. On the other hand, for the case of the smallest element separation of which the element separation is equal to the diameter of the aperture and it corresponds to the best case of the grating-lobe-problem, the ratio r_b vs the scan angle is shown in Fig. B-5 for the array elements of 2, 10, 20, and 200. The percentage of the effective aperture of an array r_u is equal to $(1-r_b)$ as shown in Equation (B-22). It is, therefore, obtained that r_u is 100% for any number of elements in an array when the array is pointed at zenith. However, when the array is pointed horizontally, r_u becomes 50% for two-element arrays, 10% for ten-element arrays, 5% for twenty-element arrays, and 0.5% for two-hundred-element arrays. The dependence of r_u on parameters N and θ' is tabulated in Table B-1.

Pointing Direction θ' \ Number of Elements N		2	10	20	200	2000
r_u%	0^o	100	100	100	100	100
	40^o	93.45	88.21	87.56	86.97	86.91
	60^o	80.45	64.81	62.86	61.10	60.92
	80^o	60.99	29.80	25.90	22.39	22.04
	90^o	50	10	5	0.5	0.05

TABLE B-1.
The effective aperture r_u in percentage for various array elements and array pointing directions with an aperture distribution of uniform amplitude and phase

The total field at observation point $P(R,\theta,\phi)$ due to a linear array of N-aperture with the arrangement in Fig. B-6 will be the sum of the contribution of the first (N-1) partially blocked apertures and the last unblocked aperture, thus

(B-23)

$$U_p = \sum_{n=0}^{N-2} U_{p_n} \text{ (partially blocked)} + U_{p_{N-1}} \text{ (unblocked)}$$

$$= \frac{j}{2\lambda} \frac{e^{-jkR}}{R} (1+\gamma)\, e^{jkz_o\gamma} \cdot$$

$$\cdot \left[\sum_{n=0}^{N-2} e^{jk\ nd \sin\theta \sin\phi}\right](I - I_b)$$

$$+ \frac{j}{2\lambda} \frac{e^{-jkR}}{R} (1+\gamma) e^{jkz_o\gamma}\, e^{jk(N-1)d \sin\theta \sin\phi} \cdot I$$

$$= \frac{j}{2\lambda} \frac{e^{-jkR}}{R} (1+\gamma) e^{jkz_o\gamma} \cdot$$

$$\cdot \left\{ I \left[\sum_{n=0}^{N-1} e^{jk\ nd \sin\theta \sin\phi}\right] - I_b \left[\sum_{n=0}^{N-2} e^{jk\ nd \sin\theta \sin\phi}\right]\right\}$$

where the factors I and $\sum_{n=0}^{N-1} e^{jk\ nd \sin\theta \sin\phi}$ are the element factor and the array factor respectively for a linear array of N-paraboloid without blockage; the factors I_b and

$$\sum_{N=0}^{N-2} e^{jk\ nd \sin\theta \sin\phi}$$

are the element factor and the array factor respectively for taking into account the blockage; the factors I and I_b are given in Eqs. (B-13) and (B-14) respectively and the parameters z_o,γ are given in Eq. (B-4).

(e) Consideration of a Simple Case

In order to observe the pattern of the system in Fraunhofer region, a simple case is considered in which the array lies along y-axis and the scanning will be performed in the right corner sector of the yz-plane. For the given condition, ϕ is $\pi/2$ and ϕ' is $\pi/2$. Hence, from Eq. (B-4)

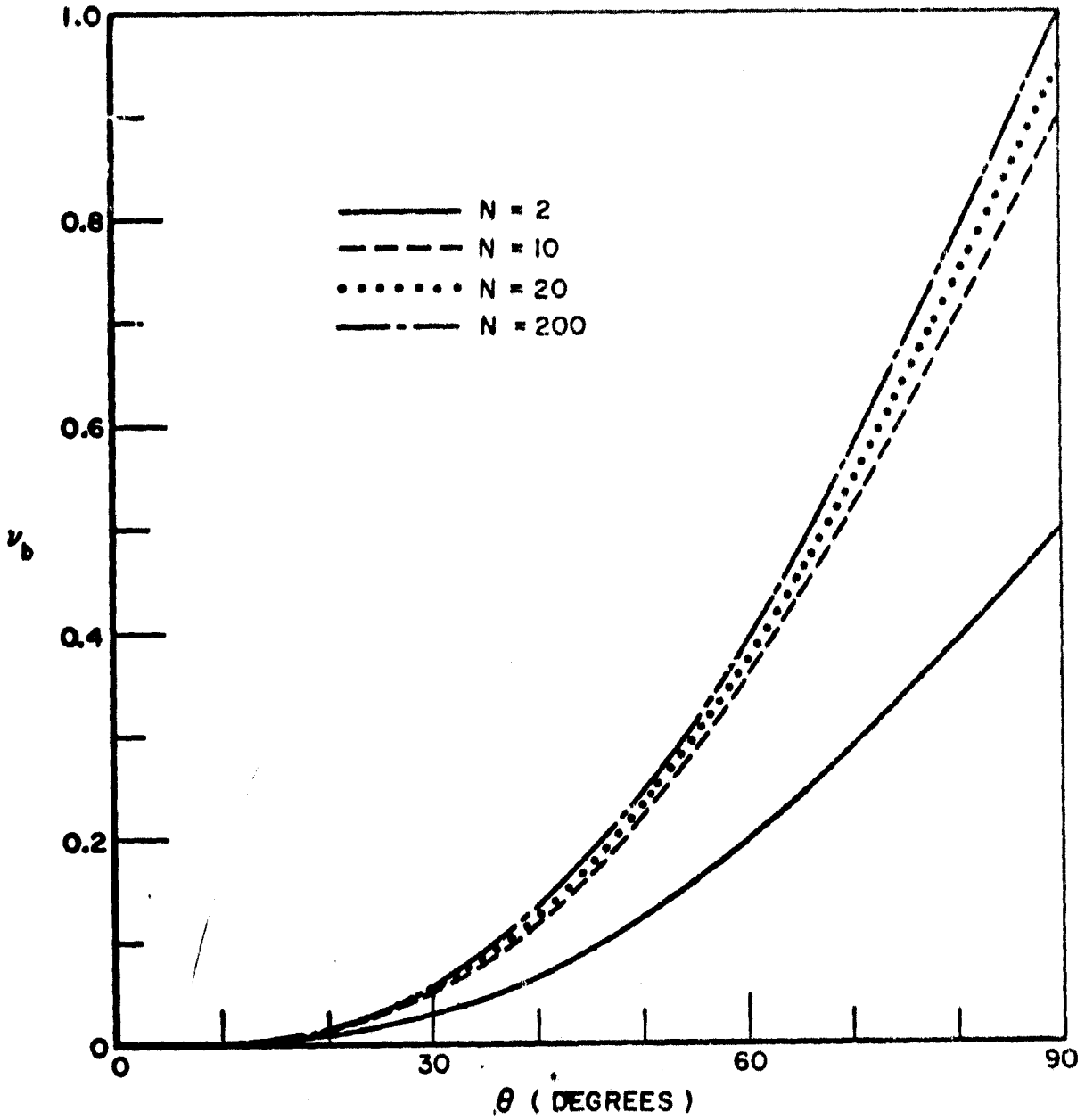
1.0
0.8
0.6
0.4
0.2
0
ν_b
N = 2
N = 10
N = 20
N = 200
0
30
60
90
θ (DEGREES)

Fig. B-5.

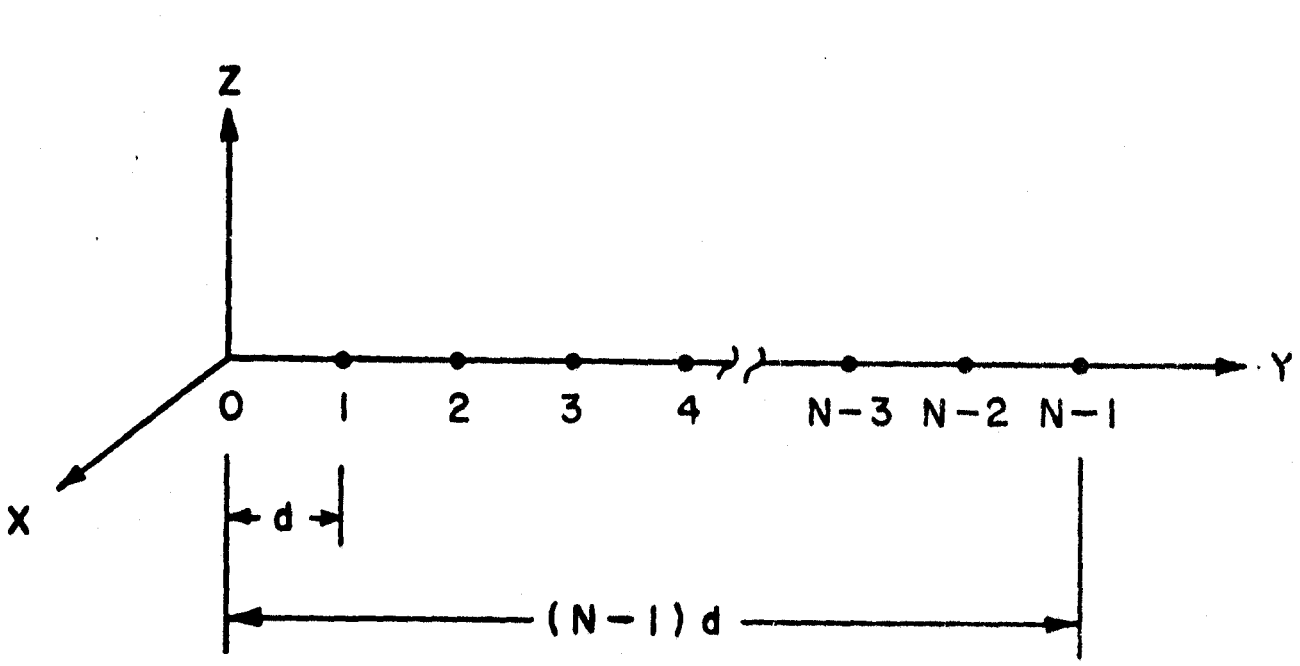
Z
Y
X
0
1
2
3
4
N-3
N-2
N-1
d
(N-1) d

Fig. B-6.

(B-24) $\gamma = \cos(\theta - \theta')$

$\alpha = \sin(\theta - \theta')$

$\beta = 0$

From Eqs. (B-8) and (B-9),

(B-25) $d' = d \cos\theta'$

(B-26) $d_\ell = 2a - d' = 2a - d\cos\theta'$

From Eqs. (B-13) and (B-14)

(B-27) $$I = \int_0^{2\pi}\int_0^{a} F(\rho,\psi)e^{jk \sin(\theta-\theta')\cos\psi}\,\rho d\rho\, d\psi$$

(B-28) $$I_b = \int_{-\Omega}^{+\Omega}\int_{\rho(\psi)}^{a} F(t,\psi)e^{jkt \sin(\theta-\theta')\cos\psi}\,\rho d\rho\, d\psi$$

For the aperture distribution $F(\rho,\psi)$, it is assumed that the feeds are normally designed to illuminate the parabolic reflectors with an intensity at the edges that is approximately 10 dB below that at center. For a tapered illumination $F(\rho,\psi)$ is given to be

(B-29) $$F(\rho,\psi) = 1 - (1-\delta)\frac{\rho^2}{a^2} \quad \text{for } \rho \leq a$$

For a 10 dB tapered illumination, the value of δ has to be 0.1.

To obtain the desired aperture distribution, in the present case, the 10 dB tapered aperture illumination, is itself an attractive problem namely aperture synthesis. For the purpose of analyzing the blocking effect of the closely spaced linear array of N-dish, it is assumed that the desired aperture distribution has been achieved without worrying about the actual technique to obtain it. The effect of tapering the illumination down toward the edge is: reduction in gain, increasing beamwidth, and reduction in side lobes as compared with the uniform aperture distribution, and reduction of the energy spilled over the edge.

The integration in Eq. (B-27) can be performed for two different cases; one is that for $\theta = \theta'$

(B-30)
$$I(\theta=\theta') = \int_0^{2\pi}\int_0^{a}\left[1 - \frac{(1-\delta)}{a^2}\rho^2\right]\rho d\rho\, d\psi = \frac{\pi a^2(1+\delta)}{2}$$

and the other one is that for $\theta \neq \theta'$, hence

(B-31)

$$I(\theta \neq \theta') = \int_0^{2\pi} \int_0^a \left[1 - \frac{(1-\delta)}{a^2}\right] \rho^2 \; e^{jk\rho \sin(\theta-\theta') \cos \psi} \; \rho d\rho \; d\psi$$
$$= 2\pi a^2 \frac{J_1(u)}{u} + 4\pi a^2 (1-\delta) \frac{J_2(u)}{u^2}$$

with

(B-32)

$$u = ka \sin(\theta-\theta').$$

The integration of I_b in Eq. (B-14) will, in general, be a complex number, hence I_b may be denoted by its real part I_{br} and imaginary part I_{bi}; thus

(B-33) $$I_b = I_{br} + j \, I_{bi}$$

and

(B-34)

$$I_{br} = \int_{-\Omega}^{+\Omega} \int_{\rho(\psi)}^a F(\rho) \cos[k\rho \sin(\theta-\theta') \cos \psi] \; \rho d\rho \; d\psi$$

(B-35)

$$I_{bi} = \int_{-\Omega}^{+\Omega} \int_{\rho(\psi)}^a F(\rho) \sin[k\rho \sin(\theta-\theta') \cos \psi] \; \rho d\rho \; d\psi$$

The integration of I_b in Eq. (B-33) can be obtained for three cases depending upon the range of the value of $d' = d \cos \theta'$. The first case is that $d' > a$, then

(B-36a)

$$I_{br}(\theta=\theta') = \frac{\Omega a^2 (1+\delta)}{2} - 2 \int_0^{+\Omega} \left[\frac{\rho_-^2}{2} - \frac{(1-\delta)}{a^2} \frac{\rho_-^4}{4}\right] d\psi$$

(B-36b) $$I_{bi}(\theta=\theta') = 0$$

where Ω is defined as the overlap angle given in Eq. (B-10) and ρ_-, one of the two roots of Eq. (B-16), is given as

(B-37) $$\rho_- = d \cos \theta' \cos \psi - \sqrt{a^2 - (d \cos \theta' \sin \psi)^2}$$

Let

(B-38a) $A = k \sin(\theta-\theta') \cos \psi$

(B-38b) $$T_1 = \frac{1}{A^2} - \frac{(1-\delta)}{a^2} \quad \frac{3A^2a^2 - 6}{A^4}$$

(B-38c) $$T_2 = \frac{a}{A} - \frac{(1-\delta)}{a^2} \quad \frac{A^2a^3 - 6a}{A^3}$$

(B-38d) $$T_3 = \frac{1}{A^2} - \frac{(1-\delta)}{a^2} \quad \frac{3A^2\rho_-^2 - 6}{A^4}$$

(B-38e) $$T_4 = \frac{\rho_-}{A} - \frac{(1-\delta)}{a^2} \quad \frac{A^2\rho_-^3 - 6\rho_-}{A^3}$$

(B-38f) $$T_5 = -\frac{1}{A^2} - \frac{(1-\delta)}{a^2} \quad \frac{6}{A^4}$$

then for $\theta \neq \theta'$,

(B-39a)

$$I_{br}(\theta\neq\theta') = 2\int_0^{+\Omega} [T_1 \cos(Aa) + T_2\sin(Aa) - T_3\cos(A\rho_-) - T_4\sin(A\rho_-)]d\psi$$

(B-39b)

$$I_{bi}(\theta\neq\theta') = 2\int_0^{+\Omega} [T_1 \sin(Aa) - T_2\cos(Aa) - T_3\sin(A\rho_-) + T_4\cos(A\rho_-)]d\psi$$

The second case is that d'=a; for this case $\Omega = \pi/3$. Hence

(B-40a)

$$I_{br}(\theta=\theta') = \frac{2a^2\pi\delta}{3} + \frac{\sqrt{3}a^2(3-7\delta)}{8}$$

(B-40b)

$$I_{bi}(\theta=\theta') = 0$$

(B-41a)

$$I_{br}(\theta\neq\theta') = 2\left[-\frac{\sqrt{3}}{k^2\sin^2(\theta-\theta')} - \frac{(1-\delta)}{a^2}\,\frac{12\sqrt{3}}{k^4\sin^4(\theta-\theta')}\right] + 2\int_0^{\Omega}[T_1\cos(Aa) + T_2\sin(Aa)]\,d\psi + 2\int_{\Omega}^{\pi/2}[T_3\cos(A\rho_+) + T_4\sin(A\rho_+) + T_5]d\psi$$

(B-41b)

$$I_{bi}(\theta\neq\theta') = 2\int_0^{\Omega}[T_1\sin(Aa) - T_2\cos(Aa)]d\psi + 2\int_{\Omega}^{\pi/2}[T_3\sin(A\rho_+) - T_4\cos(A\rho_+)]d\psi$$

where A is given in Eq. (B-38a); T_1 and T_2 are given in Eqs. (B-38b) and (B-38c) respectively; T_3 and T_4 are given in Eqs. (B-38d) and (B-38e) with ρ_- replaced by ρ_+. For d' = a case, ρ_+ is found to be

(B-42) $\rho_+ = 2a\cos\psi$

The third case is that d' < a, then

(B-43a) $$I_{br}(\theta=\theta') = \frac{\Omega a^2(1+\delta)}{2} + 2\int_{\Omega}^{\pi}\left[\frac{\rho_+^2}{2} - \frac{(1-\delta)}{a^2}\,\frac{\rho_4^4}{4}\right]d\psi$$

(B-43b) $I_{bi}(\theta=\theta') = 0$

(B-44a)

$$I_{br}(\theta\neq\theta') = 2\left[-\frac{4(1-\delta)}{a^2}\,\frac{(2+1/\cos^2\Omega)\cdot\tan\Omega}{k^4\sin^4(\theta-\theta')}\right] + 2\int_0^{\Omega}[T_1\cos(Aa) + T_2\sin(Aa)]\,d\psi + 2\int_{\Omega}^{\pi}[T_3\cos(A\rho_+) + T_4\sin(A\rho_+)]d\psi$$

(B-44b)

$$I_{bi}(\theta \neq \theta') = 2 \int_0^{\Omega} [T_1 \sin(Aa) - T_2 \cos(Aa)] d\psi$$

$$+ 2 \int_{\Omega}^{\pi} [T_3 \sin(A\rho_+) - T_4 \cos(A\rho_+)] d\psi$$

Again, A is given in Eq. (B-38a); T_1 and T_2 are given in Eqs. (B-38b) and (B-38c) respectively; T_3 and T_4 are given in Eqs. (B-38d) and (B-38e) with ρ_- replaced by ρ_+; for d' < a case, ρ_+ is found to be

(B-45) $$\rho_+ = d \cos\theta' \cos\psi + \sqrt{a^2 - (d \cos\theta' \sin\psi)^2}$$

where

θ' = the array pointing angle or the scan angle

a = radius of the circular aperture

d = separation between the adjacent paraboloids

$$k = \frac{2\pi}{\lambda}$$

The array factors in Eq. (B-23) for $\phi = \pi/2$ case are

$$\sum_{n=0}^{N-1} e^{jknd \sin\theta} = \frac{\sin \frac{kNd \sin\theta}{2}}{\sin \frac{kd \sin}{2}} e^{j \frac{k(N-1)d \sin\theta}{2}}$$

$$\sum_{n=0}^{N-2} e^{jknd \sin\theta} = \frac{\sin \frac{k(N-1)d \sin\theta}{2}}{\sin \frac{kd \sin\theta}{2}} e^{j \frac{k(N-2)d \sin\theta}{2}}$$

Let

(B-46a) $$F_1(\theta) = \frac{\sin \frac{kNd \sin\theta}{2}}{\sin \frac{kd \sin\theta}{2}}$$

(B-46b) $$F_2(\theta) = \frac{\sin \frac{k(N-1)d \sin\theta}{2}}{\sin \frac{kd \sin\theta}{2}}$$

Therefore, the total field U_p at observation point in Eq. (B-23) becomes

(B-47)

$$U_p = \frac{j}{2\lambda} \frac{e^{-jkR}}{R} (1+\gamma) e^{jkz_o\gamma} \cdot \left\{ F_1(\theta)\, I\, e^{j\frac{k(N-1)d \sin\theta}{2}} - F_2(\theta)\, I_b\, e^{j\frac{k(N-2)d \sin\theta}{2}} \right\}$$

The angular distribution $g(\theta,\phi)$ of U_p is

(B-48)

$$g(\theta,\phi) = (1+\gamma) \left\{ \left[F_1(\theta) I - F_2(\theta) \left(I_{br} \cos\frac{kd \sin\theta}{2} + I_{bi} \sin\frac{kd \sin\theta}{2} \right) \right]^2 + \left[F_2(\theta) \left(I_{br} \sin\frac{kd \sin\theta}{2} - I_{bi} \cos\frac{kd \sin\theta}{2} \right) \right]^2 \right\}^{1/2} \cdot e^{jkz_o\gamma + j\frac{k(N-1)d \sin\theta}{2}} \cdot e^{j \tan^{-1} \frac{F_2(\theta)\left[I_{br} \sin\frac{kd \sin\theta}{2} - I_{bi} \cos\frac{kd \sin\theta}{2} \right]}{F_1(\theta) I - F_2(\theta)\left[I_{br} \cos\frac{kd \sin\theta}{2} + I_{bi} \sin\frac{kd \sin\theta}{2} \right]}}$$

Let the amplitude and phase distributions of $g(\theta,\phi)$ be denoted by $A(\theta,\phi)$ and $\Psi(\theta,\phi)$ respectively, then

(B-49) $\quad g(\theta,\phi) = A(\theta,\phi)\, e^{j\Psi(\theta,\phi)}$

with

(B-50a)

$$A(\theta,\phi) = (1+\gamma) \left\{ \left[F_1(\theta) I - F_2(\theta) \left(I_{br} \cos\frac{kd \sin\theta}{2} + I_{bi} \sin\frac{kd \sin\theta}{2} \right) \right]^2 + \left[F_2(\theta) \left(I_{br} \sin\frac{kd \sin\theta}{2} - I_{bi} \cos\frac{kd \sin\theta}{2} \right) \right]^2 \right\}^{1/2}$$

(B-50b)

$$\Psi(\theta,\phi) = kz_o\gamma + \frac{k(N-1)d \sin\theta}{2} + \tan^{-1} \frac{F_2(\theta)\left[I_{br} \sin\frac{kd \sin\theta}{2} - I_{bi} \cos\frac{kd \sin\theta}{2} \right]}{F_1(\theta) I - F_2(\theta)\left[I_{br} \cos\frac{kd \sin\theta}{2} + I_{bi} \sin\frac{kd \sin\theta}{2} \right]}$$

where $F_1(\theta)$ and $F_2(\theta)$ are defined in Eqs. (B-46a) and (B-46b) respectively; I_{br} and I_{bi} are defined in Eqs. (B-34) and (B-35) respectively and I is defined in Eq. (B-27).

The formulation of Eq. (B-48) is the linear sum of N individual element signals of the array without adding any signal processing. It is found that the beam maximum is not at the direction where the array pointing direction (θ',ϕ') is. This is due to the fact that when the scan is performed, signal path difference is introduced for individual aperture in addition to the blockage. For a means of tracking and communication, it is desirable to have the beam maximum of the array coincident with the array pointing direction. To achieve this goal, the transmitting or receiving signal of each element must be compensated for phase difference with respect to a reference phase, both for phases introduced by signal path and the blockage, in order to add the signals in phase at the observation point in space or at summing point at receiving terminal.

For the simple case considered in this section, the field of the mth-element at point $P(R,\theta,\phi)$ is

$$(B\text{-}51) \qquad U_m(P) = \frac{j}{2\lambda} \frac{e^{-jkR}}{R} (1+\gamma) e^{jkz_o\gamma} e^{jk(m-1)d \sin\theta} \cdot [I - I_b]$$

The numbering of the elements in the array in Eq. (B-51) is shown below.

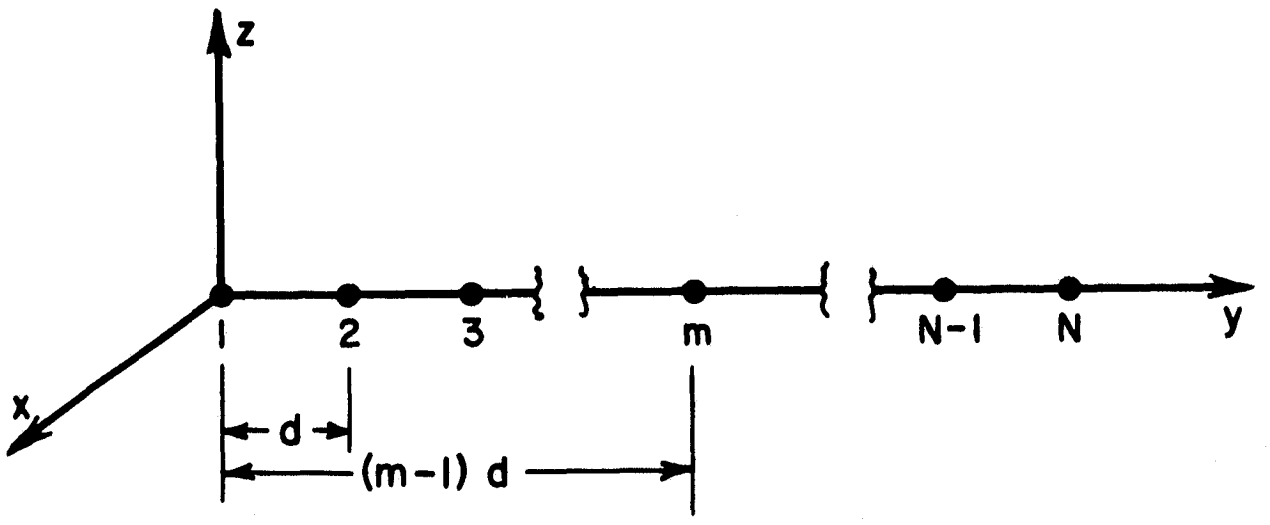

Substituting Eqs. (B-24) and (B-33) into (B-51), it yields

$$(B\text{-}52) \qquad U_m(P) = \frac{1}{2\lambda} \cdot \frac{1}{R} \left[1+\cos(\theta-\theta')\right] \left[(I-I_{br})^2 + I_{bi}^2\right]^{1/2} \cdot e^{j\pi/2} e^{-jkR} \cdot e^{jkz_o\cos(\theta-\theta')} e^{jk(m-1)d \sin\theta} e^{j \tan^{-1}\left(\frac{-I_{bi}}{I-I_{br}}\right)}$$

In order that the fields due to each element in the array are in phase at the observation point $P(R,\theta,\phi)$, it is necessary to introduce a phase factor Φ_m for the mth-element in the array to compensate the signal path and blockage resulted from scanning. The phase factor Φ_m introduced in the circuit associated with the mth element can be found from Eq. (B-52) as

(B-53)

$$\Phi_m = -\left[kz_o \cos(\theta-\theta') + k(m-1)d \sin\theta + \tan^{-1}\left(\frac{-I_{bi}}{I-I_{br}}\right)\right]$$

where z_o, I, I_{br}, and I_{bi} are given in Eqs. (B-4), (B-27), (B-34) and (B-35) respectively. It is noted in Eq. (B-53) that for the partly blocked element, in addition to the phase introduced by the signal path, there is this phase contribution resulting from the blockage.
The last element in the array is not blocked, hence its field at the observation point $P(R,\theta,\phi)$ is

(B-54)

$$\begin{aligned} U_N(P) &= \frac{j}{2\lambda}\ \frac{e^{-jkR}}{R}\ (1+\gamma)\ e^{jkz_o\gamma}\ e^{jk(N-1)d \sin\theta}\ .\ I \\ &= \frac{1}{2\lambda}\ \frac{1}{R}\ [1 + \cos(\theta-\theta')]\ I\ e^{j\pi/2}\ e^{-jkR} \\ &\quad \cdot\ e^{jkz_o \cos(\theta-\theta')}\ e^{jk(N-1)d \sin\theta} \end{aligned}$$

Consequently, the phase factor for the last element becomes

(B-55) $$\Phi_N = -[kz_o \cos(\theta-\theta') + k(N-1)d \sin\theta]$$

The total field, at point $P(R,\theta,\phi)$ in space, of an array of N-element with phase compensation for each element in the array is then the linear sum of the first (N-1) processed signals with blockage and the Nth processed signal without blockage; it is found to be

(B-56) $$U_p = \frac{j}{2\lambda}\ \frac{e^{-jkR}}{R}\ [1 + \cos(\theta-\theta')]\ \left[(N-1)\sqrt{(I-I_{br})^2 + I_{bi}^2} + I\right]$$

3) The Blocking Effect of a Closely Spaced Array Employing the Geometrical Theory of Diffraction

(a) Introduction

The formulation in the previous sections are based only upon the geometrical optics theory (geometrical ray theory). The geometrical optics theory is accurate only as the operating wavelength approaches zero; nevertheless it is a valid high frequency approximation. The first correction term to the geometrical ray approximation can be obtained by employing the geometrical theory of diffraction (GTD) de-

veloped by Keller (Ref. B-3, B-4). The geometrical theory of diffraction is an extension of the geometrical ray theory to take into account the fields produced by the incident rays which hit edges, vertices of boundary surfaces, or which graze such surfaces. The geometrical theory of diffraction is a valid high frequency approximation in complement with the geometrical ray theory. It has been shown, for example edge diffraction from truncated paraboloids and hyperboloids (Ref. B-5,6), diffraction by a cylinder of any cross section (Ref. B-7), diffraction by a smooth three-dimensional object of any shape (Ref. B-8) and other diffraction problems (Ref. B-3,9), that the technique employing both the geometrical ray theory and the geometrical theory of diffraction predicts successfully the radiation pattern for various shapes of scattering bodies. In these cases, excellent agreement between GTD results and previously known exact results have been obtained. It is found that GTD results agreed perfectly with the leading terms in the asymptotic expansion of the exact solutions of the diffraction problems, the expansion being with respect to the wave number $k = 2\pi/\lambda$, as k approaches infinity. The technique of ray tracing is employed in the geometrical theory of diffraction. It has been shown that it gives even better results when additional higher order diffracted rays (multiple diffracted rays), such as doubly diffracted, triply diffracted, ..., and nth order diffracted rays, are taken into account (Ref. B-3,4). The basic formulation of the theory of GTD can be found elsewhere, for example Reference 4, it will not be repeated here.

For a parabolic reflector with a focal feed, there are edge-diffracted rays generated by the incident ray which hits the edge of the parabolic reflector. These edge-diffracted rays predict successfully the wide angle side lobes of a parabolic reflector antenna (Ref. B-6). For a two-element array of parabolic reflector antennas, the blocked reflector is generally in the wide angle side lobe region of the unblocked one when the scanning is performed. Thus the edge-diffracted rays generated by the unblocked reflector are partly collected by the blocked reflector. It is then the interaction between the neighboring parabolic reflectors can be investigated.

In the geometrical optics approximation as investigated in Sec. 2, the contribution to the aperture distribution is assumed to come solely from the feed. Considering the edge diffraction mechanism, the contribution to the aperture distribution of a blocked reflector is the sum of the following two types of edge diffracted rays in addition to the direct ray from the feed: rays generated by the unblocked reflector and rays generated by the edge of the same blocked reflector. For the unblocked reflector, the contribution will be the direct ray from its feed and the edge diffracted ray from its aperture edge.

Both the current and aperture distribution methods can be used to predict the radiation pattern in the forward axial region of an array. To obtain the wide angle radiation pattern of an array, the reflected rays reflected by a convex surface of a reflector must be included.

The field associated with the edge-diffracted ray of a parabolic reflector is obtained in Sec. 3b. The surface current distribution on a paraboloidal surface due to the direct ray from its primary feed and the edge diffracted ray from its own edge is obtained in Sec. 3c. The surface current distribution on a paraboloidal surface due to the edge diffracted ray from an adjacent reflector in an array is obtained in Sec. 3d. A brief summary is given in Sec. 3e.

b) The Field of Edged-Diffracted Rays of a Parabolic Reflector Antenna

In Fig. B-7, a parabolic reflector antenna is shown with its vertex at the origin O of the rectangular coordinate system (x',y',z') with its axis coincident with z'-axis. To describe an observation point P_o in space a spherical coordinate system $P_o(v,\xi,\delta)$ with its origin at point O is employed, where v is the distance from the origin to the observation point; ξ is the polar angle measured from z'-axis; and δ is the azimuth angle measured from x'-axis. A point Q on the paraboloidal surface can be described by a cylindrical coordinate system $Q(\rho,\delta,z')$ with its origin at point O, where ρ is the radical distance measured from z'-axis; this point Q on the surface can also be defined by a spherical coordinate system $Q(\ell,\psi,\delta)$ with its origin at the focal point F, where ℓ is the distance from the focal point to point Q; ψ is $(\pi-\theta_o)$ with θ_o being the polar angle measured from z'-axis; and again δ is the azimuth angle measured from x'-axis. The distance from the focal point to an edge point Q_i on the circular edge of a parabolic reflector is denoted by ℓ_o and the angle subtended at the focal point by a radius of the aperture is ψ_o. Let the radius of the aperture and the focal length of the parabolic reflector be denoted by "a" and "f" respectively, then an edge point can be described either as $Q_i(\ell_o,\psi_o,\delta)$ or by $Q_i(a,\delta,z_o)$ with z_o being $a^2/4f$.

The reflector is assumed to have a sharp edge and a perfectly conducting surface. The reflector is illuminated by a primary feed antenna located at the focal point. For the present analysis, the feed is assumed to be a radiator whose dimension is small compared with the aperture diameter and its pattern is assumed to be broadly directional with its maximum value coincident with the reflector axis. It is assumed that the reflector is in the far-zone region of the feed antenna; consequently the incident field at a point on the paraboloidal surface is essentially a TEM wave and its polarization can be specified in its transverse plane with respect to the propagation direction of the incident ray $\hat{I}$. At any point on the paraboloidal surface $Q(\ell,\psi,\delta)$, let the unit vectors $\hat{I}$, $\hat{e}$, and $\hat{p}$ form a set of orthonormal basis where $\hat{e}$ and $\hat{p}$ are in the transverse plane of $\hat{I}$ and $\hat{p} = \hat{e} \times \hat{I}$. It is noted $\hat{I}$ and $\hat{p}$ are in the constant δ-plane; $\hat{e}$ is perpendicular to this δ-plane. The unit vectors at point $Q(\ell,\psi,\delta)$ on the paraboloidal surface are found to be

$$\text{(B-70a)} \quad \hat{I} = \hat{x}' \sin\psi\cos\delta + \hat{y}' \sin\psi\sin\delta + \hat{z}'(-\cos\psi)$$

$$\text{(B-70b)} \quad \hat{e} = \hat{x}'(-\sin\delta) + \hat{y}'\cos\delta$$

$$\text{(B-70c)} \quad \hat{p} = \hat{x}'(-\cos\psi\cos\delta) + \hat{y}'(-\cos\psi\sin\delta) + \hat{z}'(-\sin\psi)$$

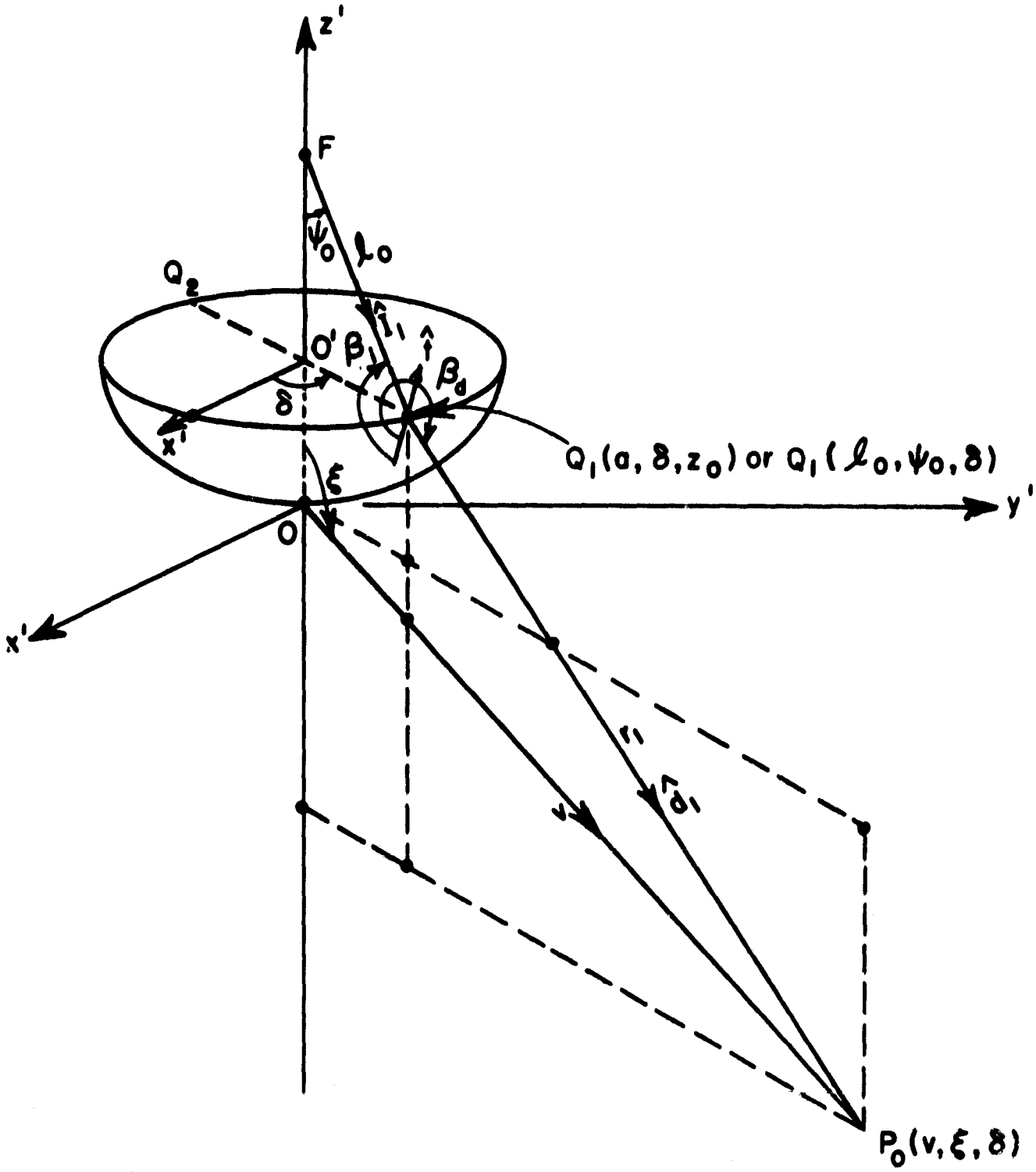
z'
F
ψ_0
ℓ_0
Q_2
O'
β_1
$\hat{i}_1$
$\hat{i}$
β_0
δ
x'
$Q_1(a, \delta, z_0)$ or $Q_1(\ell_0, \psi_0, \delta)$
ξ
y'
O
x'
r
$\hat{r}_0$
v
$P_0(v, \xi, \delta)$

Fig. B-7.

The unit vectors $\hat{X}_\delta$ and $\hat{X}_\rho$ tangent to the paraboloidal surface at point Q are given as

$$\hat{X}_\delta = \hat{e}$$

$$\hat{X}_\rho = \hat{x}' \cos\frac{\psi}{2} \cos\delta + \hat{y}' \cos\frac{\psi}{2} \sin\delta + \hat{z}' \sin\frac{\psi}{2}$$

The unit vector normal to the paraboloidal surface at point Q pointing toward the aperture is $\hat{X}_\rho \times \hat{X}_\delta$; let it be denoted by $\hat{n}$, then it can be obtained as

$$\hat{n} = \hat{x}' \left(-\sin\frac{\psi}{2} \cos\delta\right) + \hat{y}' \left(-\sin\frac{\psi}{2} \sin\delta\right) + \hat{z}' \cos\frac{\psi}{2} \tag{B-70d}$$

The polarization of the incident field at point Q on the surface can be expressed to be

$$\bar{E}^f(Q) = [\hat{e}\, A\, g(\psi,\delta) + \hat{p}\, B\, h(\psi,\delta)]\ \frac{e^{-jk\ell}}{\ell} \tag{B-71}$$

where A and B are amplitudes; $g(\psi,\delta)$ and $h(\psi,\delta)$ are angular distribution functions of the electric field at point Q on the paraboloidal surface from the primary feed antenna for $\hat{e}$ and $\hat{p}$ polarization respectively.

For an observation point $P_0(v,\xi,\delta)$ in space in Fig. B-7, consider the path from the feed to the observation point which includes a point on the edge of the reflector; the path consists of two straight line sections in a homogeneous medium. There exist two points Q_1 and Q_2 on the edge of the reflector which make the distance along the path a minimum and maximum, respectively. According to Keller's extension of Fermat's principle (Ref. B-4), both minimum and maximum paths are trajectories of two edge diffracted rays. The edge points are defined by the meridian plane which intercepts the edge of the reflector at Q_1 and Q_2.

Since high frequency diffraction is essentially a local phenomenon, the edge diffracted field can be determined in terms of the reflector and ray geometries at the point of diffraction Q_i $(i = 1,2)$ on the edge. The field of an edge diffracted ray $\bar{E}_i^d(P_0)$ at the observation point P_0 is given by (Ref. B-10).

$$\bar{E}_i^d(P_0) = \bar{\bar{D}}(Q_i) \cdot \bar{E}^f(Q_i) \sqrt{\frac{\rho_i}{r_i(\rho_i + r_i)}}\ e^{-jkr_i} \tag{B-72}$$

where $\bar{\bar{D}}$ is the dyadic diffraction coefficient for a straight edge,

$\bar{E}^f(Q_i)$ is the electric field of the feed at point Q_i on edge, $i = 1,2$,

ρ_i is the distance of the caustic from the edge at Q_i,

r_i is the distance from Q_i to the observation point P_o.

The dyadic diffraction coefficient for a straight line $\overline{\overline{D}}$ and the caustic distance ρ_i are given in Appendix I and II respectively.

From Appendix I, the dyadic diffraction coefficient at edge point Q_i with normal incidence on the edge is given to be

$$\overline{\overline{D}}(Q_i) = \hat{e}\,\hat{e}\,D_s(Q_i) + \hat{q}\,\hat{p}\,D_h(Q_i) \tag{B-73}$$

where $\hat{e}$ is the unit vector tangent to the edge at Q_i,

$\hat{p} = \hat{e} \times \hat{I}$; $\hat{I}$ being the unit vector in the direction of the incident ray,

$\hat{q} = \hat{e} \times \hat{d}$; $\hat{d}$ being the unit vector in the direction of the diffracted ray.

The scalar edge diffraction coefficients $D_s(Q_i)$ and $D_h(Q_i)$ stand for the soft and hard boundary conditions respectively; by soft boundary condition it implies that the total scalar field $u = 0$ at the edge, and for hard boundary condition, it means $\partial u/\partial n = 0$ at the edge with n being in the direction normal to the edge. The scalar diffraction coefficients $D_s(Q_i)$ and $D_h(Q_i)$ are given as

$$D_{\substack{s\\h}}(Q_i) = D_{\substack{s\\h}}(\beta_d(Q_i), \beta_i(Q_i)) \tag{B-74}$$

$$= \frac{-e^{-j\frac{\pi}{4}}}{2\sqrt{2\pi k}} \left[\frac{F(kL_i a_-)}{\cos\frac{\beta_d - \beta_i}{2}} \mp \frac{F(kL_i a_+)}{\cos\frac{\beta_d + \beta_i}{2}} \right]$$

with

$$a_{\mp} = 1 + \cos(\beta_d \mp \beta_i), \tag{B-75}$$

$$F(kL_i a_{\mp}) = j2\sqrt{kL_i a_{\mp}}\; e^{jkL_i a_{\mp}} \cdot \int_{\sqrt{kL_i a_{\mp}}}^{\infty} e^{-j\tau^2}\, d\tau\,, \tag{B-76}$$

$$L_i = \frac{r_i \ell_o}{r_i + \ell_o} \quad \text{for spherical wave,} \tag{B-77}$$

ℓ_o is the distance from the focal point to point Q_i on the edge.

It is seen that the dyadic diffraction coefficient $\bar{\bar{D}}$ is a function of the incident and diffracted ray geometries at the point of diffraction Q_i on the edge; it does not depend on the edge curvature. The curvature of the edge is taken into account by the divergence factor,

$$\left[\frac{\rho_i}{r_i(\rho_i+r_i)}\right]^{1/2}$$

which is expressed in terms of the caustic distance at the edge.

The Edge Diffracted Field $\bar{E}_1^d(P_0)$ at the Observation Point $P_0(v,\xi,\delta)$ Due to the Diffraction at Edge Point Q_1

In Fig. B-7, at edge point $Q_1(a,\delta,z_0)$ the unit vectors in Eqs. (B-70) and (B-73) are obtained to be

(B-80)

$$\hat{e}_1 = \hat{x}'(-\sin\delta) + \hat{y}'\cos\delta$$

$$\hat{I}_1 = \hat{x}'\sin\Psi_0\cos\delta + \hat{y}'\sin\Psi_0\sin\delta + \hat{z}'(-\cos\Psi_0)$$

$$\hat{p}_1 = \hat{x}'(-\cos\Psi_0\cos\delta) + \hat{y}'(-\cos\Psi_0\sin\delta) + \hat{z}'(-\sin\Psi_0)$$

$$\hat{d}_1 = \hat{x}'\frac{(v\sin\xi - a)\cos\delta}{r_1} + \hat{y}'\frac{(v\sin\xi - a)\sin\delta}{r_1} + z'\frac{(v\cos\xi - z_0)}{r_1}$$

$$\hat{q}_1 = x'\frac{(v\cos\xi - z_0)\cos\delta}{r_1} + \hat{y}'\frac{(v\cos\xi - z_0)\sin\xi}{r_1} + \hat{z}'\frac{-(v\sin\xi - a)}{r_1}$$

$$\hat{n}_{e1} = \hat{x}'\cos\delta + \hat{y}'\sin\delta$$

$$\hat{t}_1 = x'\frac{\cos\delta}{\sqrt{1+\left(\frac{a}{2f}\right)^2}} + \hat{y}'\frac{\sin\delta}{\sqrt{1+\left(\frac{a}{2f}\right)^2}} + \hat{z}'\frac{\frac{a}{2f}}{\sqrt{1+\left(\frac{a}{2f}\right)^2}}$$

with

(B-81) $$r_1 = [(v\sin\xi - a)^2 + (v\cos\xi - z_0)^2]^{1/2}$$

(B-82) $$z_0 = \frac{a^2}{4f}\ ;\quad \Psi_0 = \tan^{-1}\frac{a}{f - z_0}$$

The unit vector $\hat{n}_{e1}$ is defined in Appendix II and $\hat{t}$ is the unit vector tangent to the paraboloidal surface at edge point Q_1 in the constant δ-plane. It is noted that the unit vectors $\hat{e}_1$ and $\hat{p}_1$ are in the transverse plane of $\hat{I}_1$; the unit vectors $\hat{e}_1$ and $\hat{q}_1$ are in the transverse plane of $\hat{d}_1$. From Appendix II, the divergence factor at edge point Q_1 is found to be

(B-83) $$\sqrt{\frac{\rho_1}{r_1(\rho_1+r_1)}} = \frac{1}{\sqrt{r_1}}\sqrt{\frac{a}{v \sin \xi}}$$

The incident field at edge point Q_1 is given in Eq. (B-71) to be

(B-84) $$\bar{E}^f(Q_1) = \hat{e}_1 E_e^f(Q_1) + \hat{p}_1 E_p^f(Q_1)$$

with

(B-84a) $$E_e^f(Q_1) = A\, g(\psi_o,\delta)\, \frac{e^{-jk\ell_o}}{\ell_o}$$

(B-84b) $$E_p^f(Q_1) = Bh(\psi_o,\delta)\, \frac{e^{-jk\ell_o}}{\ell_o}$$

Substituting Eqs. (B-83), (B-82), (B-80), (B-74), and (B-73) into (B-72), the field of the edge diffracted ray $\bar{E}_1^d(P_o)$ becomes

(B-85) $$\bar{E}_1^d(P_o) = \hat{e}_1 E_{e1}^d(P_o) + \hat{q}_1 E_{q1}^d(P_o)$$

where $E_{e1}^d(P_o)$ and $E_{q1}^d(P_o)$ are two components, in the transverse plane of the ray direction, of the edge diffracted rays originated at edge point Q_1; they are found to be

(B-85a)

$$E_{e1}^d(P_o) = E_e^f(Q_1)\, D_s(Q_1)\sqrt{\frac{\rho_1}{r_1(\rho_1+r_1)}}\, e^{-jkr_1}$$

$$= E_e^f(Q_1) \cdot \frac{-e^{-j\frac{\pi}{4}}}{2\sqrt{2\pi k}}$$

$$\cdot\left[\frac{F(kL_1 a_-(Q_1))}{\cos\frac{\beta_d(Q_1)-\beta_i(Q_1)}{2}} - \frac{F(kL_1 a_+(Q_1))}{\cos\frac{\beta_d(Q_1)+\beta_i(Q_1)}{2}}\right]$$

$$\cdot \frac{1}{\sqrt{r_1}}\sqrt{\frac{a}{v \sin \xi}}\, e^{-jkr_1}$$

(B-85b)

$$E^d_{q1}(P_o) = E^f_p(Q_1)\, D_h(Q_1) \sqrt{\frac{\rho_1}{r_1(\ell_1 + r_1)}}\, e^{-jkr_1}$$

$$= E^f_p(Q_1) \cdot \frac{-e^{-j\frac{\pi}{4}}}{2\sqrt{2\pi k}}$$

$$\cdot \left[\frac{F(kL_1 a_-(Q_1))}{\cos \frac{\beta_d(Q_1) - \beta_i(Q_1)}{2}} + \frac{F(kL_1 a_+(Q_1))}{\cos \frac{\beta_d(Q_1) + \beta_i(Q_1)}{2}} \right]$$

$$\cdot \frac{1}{r_1} \sqrt{\frac{a}{v \sin \xi}}\, e^{-jkr_1}$$

with

(B-85c) $$a_-(Q_1) = 1 + \cos[\beta_d(Q_1) - \beta_i(Q_1)]$$

(B-85d) $$a_+(Q_1) = 1 + \cos[\beta_d(Q_1) + \beta_i(Q_1)]$$

(B-85e) $$L_1 = \frac{r_1 \ell_o}{r_1 + \ell_o}$$

(B-85f) $$F(kL_1 a_{\mp}(Q_1)) = j\, 2\sqrt{kL_1 a_{\mp}(Q_1)}\, e^{jkL_1 a_{\mp}(Q_1)} \cdot$$

$$\cdot \int_{\sqrt{kL_1 a_{\mp}(Q_1)}}^{\infty} e^{-j\tau^2} d\tau$$

The incident angle $\beta_i(Q_1)$ is found to be

(B-86) $$\beta_i(Q_1) = \frac{\pi}{2} - \psi_o + \tan^{-1}\left(\frac{a}{2f}\right)$$

To obtain the diffracted angle $\beta_d(Q_1)$, there are five regions to be considered. The difference and sum of the incident and diffracted angles, $\beta_d(Q_1)$ and $\beta_i(Q_1)$, are given in these five regions in Table B-2.

TABLE B-2

Region	Range of $\beta_d(Q_1)$	$\beta_d(Q_1)-\beta_i(Q_1)$	$\beta_d(Q_1)+\beta_i(Q_1)$
1	$0 < \beta_d < \Gamma_o$	$\tan^{-1} \frac{\frac{a}{2f}(v \sin \xi - a) - (v \cos \xi - z_o)}{(v \sin \xi - a) + \frac{a}{2f}(v \cos \xi - z_o)}$ $-\Gamma_o - \frac{\pi}{2} + \Psi_o$	$\tan^{-1} \frac{\frac{a}{2f}(v \sin \xi - a) - (v \cos \xi - z_o)}{(v \sin \xi - a) + \frac{a}{2f}(v \cos \xi - z_o)}$ $+ \Gamma_o + \frac{\pi}{2} - \Psi_o$
2	$\Gamma_o < \beta_d < \Gamma_o + \frac{\pi}{2}$	$\tan^{-1} \frac{v \cos \xi - z_o}{v \sin \xi - a} - \frac{\pi}{2} + \Psi_o$	$\tan^{-1} \frac{v \cos \xi - z_o}{v \sin \xi - a} + 2\Gamma_o + \frac{\pi}{2} - \Psi_o$
3	$\Gamma_o + \frac{\pi}{2} < \beta_d < \Gamma_o + \pi$	$\tan^{-1} \frac{v \sin \xi - a}{v \cos \xi - z_o} + \Psi_o$	$\tan^{-1} \frac{v \sin \xi - a}{v \sin \xi - z_o} + 2\Gamma_o + \pi - \Psi_o$
4	$\Gamma_o + \pi < \beta_d < \Gamma_o + \frac{3\pi}{2}$	$\tan^{-1} \frac{v \cos \xi - z_o}{v \sin \xi - a} + \frac{\pi}{2} + \Psi_o$	$\tan^{-1} \frac{v \cos \xi - z_o}{v \sin \xi - a} + 2\Gamma_o + \frac{3\pi}{2} - \Psi_o$
5	$\frac{3\pi}{2} + \Gamma_o < \beta_d < 2\pi$	$\tan^{-1} \frac{v \sin \xi - a}{-(v \cos \xi - z_o)} + \pi + \Psi_o$	$\tan^{-1} \frac{v \sin \xi - a}{-(v \cos \xi - z_o)} + 2\Gamma_o + 2\pi - \Psi_o$

The parameter Γ_o, the angle between the unit vectors $-\hat{t}(Q_1)$ and $-\hat{n}_e(Q_1)$, is given as

(B-87) $$\Gamma_o = \tan^{-1}\frac{a}{2f}$$

The angle Ψ_o is the angle subtended at the focal point by a radius of the aperture. For the values of $\beta_d(Q_1)$ at the boundaries, the difference and sum of $\beta_d(Q_1)$ and $\beta_i(Q_1)$ are given in Table B-3 below.

TABLE B-3

$\beta_d(Q_1)$	$\beta_d(Q_1) - \beta_i(Q_1)$	$\beta_d(Q_1) + \beta_i(Q_1)$
0	$-\Gamma_o - \frac{\pi}{2} + \Psi_o$	$\Gamma_o + \frac{\pi}{2} - \Psi_o$
Γ_o	$-\frac{\pi}{2} + \Psi_o$	$2\Gamma_o + \frac{\pi}{2} - \Psi_o$
$\Gamma_o + \frac{\pi}{2}$	Ψ_o	$2\Gamma_o + \pi - \Psi_o$
$\Gamma_o + \pi$	$\frac{\pi}{2} + \Psi_o$	$2\Gamma_o + \frac{3\pi}{2} - \Psi_o$
$\Gamma_o + \frac{3\pi}{2}$	$\pi + \Psi_o$	$2\Gamma_o + \pi - \Psi_o$
2π	$-\Gamma_o + \frac{3\pi}{2} + \Psi_o$	$\Gamma_o + \frac{5\pi}{2} - \Psi_o$

The Edge Diffracted Field $\bar{E}_2^d(P_o)$ at the Observation Point $P_o(v,\xi,\delta)$ Due to the Diffraction at the Edge Point Q_2

In Fig. B-8, the unit vectors associated with edge point $Q_2(a,\pi+\delta,z_o)$ are obtained as

(B-88)

$$\hat{e}_2 = \hat{x}'\ \sin\delta + \hat{y}'\ (-\cos\delta)$$

$$\hat{I}_2 = \hat{x}'\ (-\sin\Psi_o\cos\delta) + \hat{y}'\ (-\sin\Psi_o\sin\delta) + \hat{z}'\ (-\cos\Psi_o)$$

$$\hat{p}_2 = \hat{x}'\ \cos\Psi_o\cos\delta + \hat{y}'\ \cos\Psi_o\sin\delta + \hat{z}'\ (-\sin\Psi_o)$$

$$\hat{d}_2 = \hat{x}'\ \frac{(v\sin\xi + a)\cos\delta}{r_2} + \hat{y}'\ \frac{(v\sin\xi + a)\sin\delta}{r_2} + \hat{z}'\ \frac{(v\cos\xi - z_o)}{r_2}$$

$$\hat{q}_2 = \hat{x}'\ \frac{-(v\cos\xi - z_o)\cos\delta}{r_2} + \hat{y}'\ \frac{-(v\cos\xi - z_o)\sin\delta}{r_2} + \hat{z}'\ \frac{(v\sin\xi + a)}{r_2}$$

$$\hat{n}_{e2} = \hat{x}'\ (-\cos\xi) + \hat{y}'\ (-\sin\delta)$$

$$\hat{t}_2 = x'\ \frac{-\cos\delta}{\sqrt{1 + (a/2f)^2}} + \hat{y}'\ \frac{-\sin\delta}{\sqrt{1 + (a/2f)^2}} + z'\ \frac{\frac{a}{2f}}{\sqrt{1 + (a/2f)^2}}$$

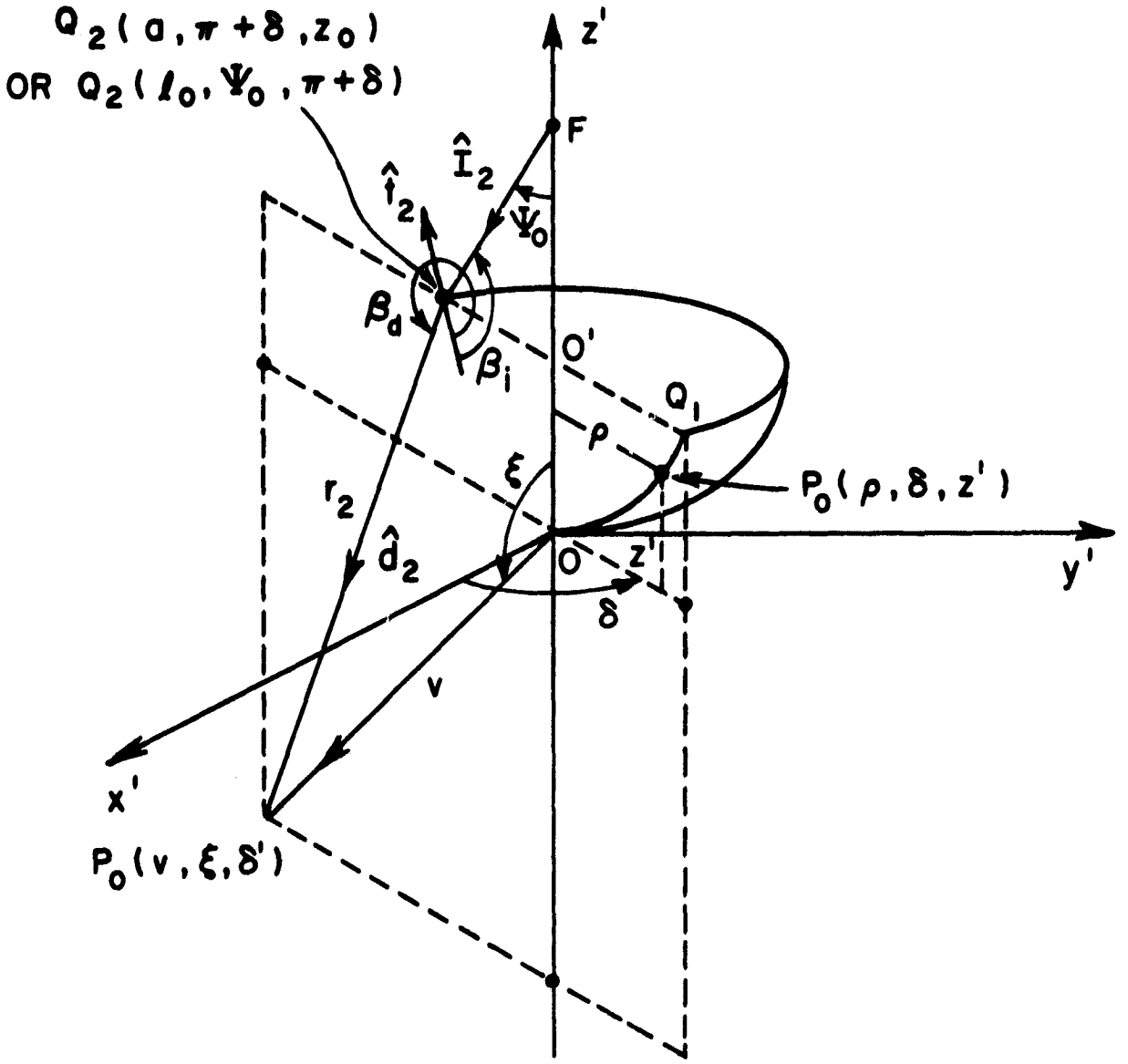

Fig. B-8.

with

$$r_2 = [(v \sin \xi + a)^2 + (v \cos \xi - z_0)^2]^{1/2} \tag{B-89}$$

and z_0 is given in Eq. (B-82). Again, it is noted that the unit vectors $\hat{e}_2$ and $\hat{p}_2$ are in the transverse plane of $\hat{I}_2$; the unit vectors $\hat{e}_2$ and $\hat{q}_2$ are in the transverse plane of $\hat{d}_2$. The divergence factor at edge point Q_2 is found to be

$$\sqrt{\frac{\rho_2}{r_2(\rho_2+r_2)}} = \frac{j}{\sqrt{r_2}} \sqrt{\frac{a}{v \sin \xi}} \tag{B-90}$$

As the incident field at edge point Q_2 given as

$$\text{(B-91)} \qquad \bar{E}^f(Q_2) = \hat{e}_2 \, E_e^f(Q_2) + \hat{p}_2 \, E_p^f(Q_2)$$

with

$$\text{(B-91a)} \qquad E_e^f(Q_2) = A \, g(\Psi_o, \pi+\delta) \, \frac{e^{-jk\ell_o}}{\ell_o}$$

$$\text{(B-91b)} \qquad E_p^f(Q_2) = B \, h(\Psi_o, \pi+\delta) \, \frac{e^{-jk\ell_o}}{\ell_o}$$

the field of the diffracted ray $\bar{E}_2^d(P_o)$ at observation point $P_o(v,\xi,\delta)$ becomes

$$\text{(B-92)} \qquad \bar{E}_2^d(P_o) = \hat{e}_2 \, E_{e2}^d(P_o) + \hat{q}_2 \, E_{q2}^d(P_o)$$

where

(B-92a)

$$E_{e2}^d(P_o) = E_e^f(Q_2) \, D_s(Q_2) \sqrt{\frac{\rho_2}{r_2(r_2+\rho_2)}} \, e^{-jkr_2}$$

$$= E_e^f(Q_2) \cdot \frac{-e^{-j\frac{\pi}{4}}}{2\sqrt{2\pi k}}$$

$$\cdot \left[\frac{F(kL_2 a_-(Q_2))}{\cos \frac{\beta_d(Q_2)-\beta_i(Q_2)}{2}} - \frac{F(kL_2 a_+(Q_2))}{\cos \frac{\beta_d(Q_2)+\beta_i(Q_2)}{2}} \right]$$

$$\cdot \frac{j}{\sqrt{r_2}} \sqrt{\frac{a}{v \sin \xi}} \, e^{-jkr_2}$$

(B-92b)

$$E^d_{q2}(P_o) = E^f_p(Q_2)\, D_h(Q_2)\sqrt{\frac{\rho_2}{r_2(\rho_2+r_2)}}\; e^{-jkr_2}$$

$$= E^f_p(Q_2)\cdot\frac{-e^{-j\frac{\pi}{4}}}{2\sqrt{2\pi k}}$$

$$\cdot\left[\frac{F(kL_2a_-(Q_2))}{\cos\frac{\beta_d(Q_2)-\beta_i(Q_2)}{2}} + \frac{F(kL_2a_+(Q_2))}{\cos\frac{\beta_d(Q_2)+\beta_i(Q_2)}{2}}\right]$$

$$\cdot\frac{j}{\sqrt{r_2}}\sqrt{\frac{a}{v\sin\xi}}\; e^{-jkr_2}$$

with

(B-92c) $\quad a_-(Q_2) = 1 + \cos[\beta_d(Q_2) - \beta_i(Q_2)]$

(B-92d) $\quad a_+(Q_2) = 1 + \cos[\beta_d(Q_2) + \beta_i(Q_2)]$

(B-92e) $\quad L_2 = \dfrac{r_2\ell_o}{r_2+\ell_o}$

(B-92f) $\quad F(kL_2a_\mp(Q_2) = j\,2\sqrt{kL_2a_\mp(Q_2)}\; e^{jkL_2a_\mp(Q_2)}$

$$\cdot\frac{\int_{\sqrt{kL_2a_\mp(Q_2)}}^{\infty} e^{-j\tau^2}\,d\tau}{}$$

The incident angle $\beta_i(Q_2)$ is found to be the same as $\beta_i(Q_1)$ as given in Eq. (B-86). Also there are five regions to be considered to obtain the diffracted angle at edge point $\beta_d(Q_2)$. The difference and sum of the diffracted and incident angle, $\beta_d(Q_2)-\beta_i(Q_2)$ and $\beta_d(Q_2)+\beta_i(Q_2)$, respectively are given in Table B-2 and B-3 with term $(v \sin\xi - a)$ replaced by $(v \sin\xi + a)$.

It is obvious the total edge diffracted field at the observation point $P_o(v,\xi,\delta)$ is the sum of the fields which are edge diffracted at Q_1 and Q_2. However, over a certain range of angle ξ, the contribution to the edge diffracted field at point P_o comes only from one of the two edge diffracted rays as the other one blocked by the paraboloidal surface.

Thus, the total edge diffracted field at point P_o is

$$\text{(B-93)} \qquad \bar{E}^d(P_o) = \begin{cases} \bar{E}_1^d(P_o) + \bar{E}_2^d(P_o) & P_o \text{ visible from } Q_1 \text{ and } Q_2 \\ \bar{E}_1^d(P_o) & P_o \text{ visible from } Q_1 \text{ only} \\ \bar{E}_2^d(P_o) & P_o \text{ visible from } Q_2 \text{ only} \end{cases}$$

The range of the diffracted angle $\beta_d(Q_i)$ in which the edge diffracted ray generated at edge point Q_i illuminates can be found as follows:

For the observation points on the paraboloidal surface inside the region bounded by the parabolic reflector and its surface, the range of $\beta_d(Q_i)$ at edge point Q_i is

$$\text{(B-94)} \qquad 0 < \beta_d(Q_i) < \Gamma_o$$

For the observation outside the region mentioned above, the range of the diffracted angle $\beta_d(Q_i)$ in which the edge diffracted ray $\bar{E}_i^d(P_o)$ is not shadowed by the paraboloidal surface is

$$\text{(B-95)} \qquad \Gamma_o < \beta_d(Q_i) - \Gamma_o < \frac{3\pi}{2} + \tan^{-1}\left(\frac{2f}{a}\right)$$

where Γ_o is the angle between $-\hat{n}_e(Q_i)$ and $-\hat{t}(Q_i)$ given in Eq. (B-87).

(c) Surface Current Distribution of a Parabolic Reflector Antenna with Both the Contributions from the Feed and the Edge Diffracted Rays

In Fig. B-9, it shows a single parabolic reflector antenna with its vertex at the origin of the rectangular coordinate system (x',y',z') and its axis coincident with the z'-axis. A point P_o on the paraboloidal surface can be defined by a spherical coordinate system with its origin at the focal point F as $P_o(\ell,\psi,\delta)$ where ℓ is the distance from the focal point to point P_o; ψ is $(\pi-\theta_o)$ with θ_o being the polar angle measured from z'-axis; δ is the azimuth angle measured from x'-axis.

At point P_o, in addition to the direct ray from the feed there exist two edge diffracted rays originated at edge points $Q_1(a,\delta, z_o)$ and $Q_2(a,\pi+\delta,z_o)$ which are defined by points of intersection of the constant δ-plane and the circular edge of the parabolic reflector. The current density induced on the paraboloidal surface due to both edge diffracted rays from its own circular edge becomes the first correction factor to the primary current density induced by the direct ray from its feed. In the text to follow, the surface current contributions due to both the direct ray and the edge diffracted rays will be formulated.

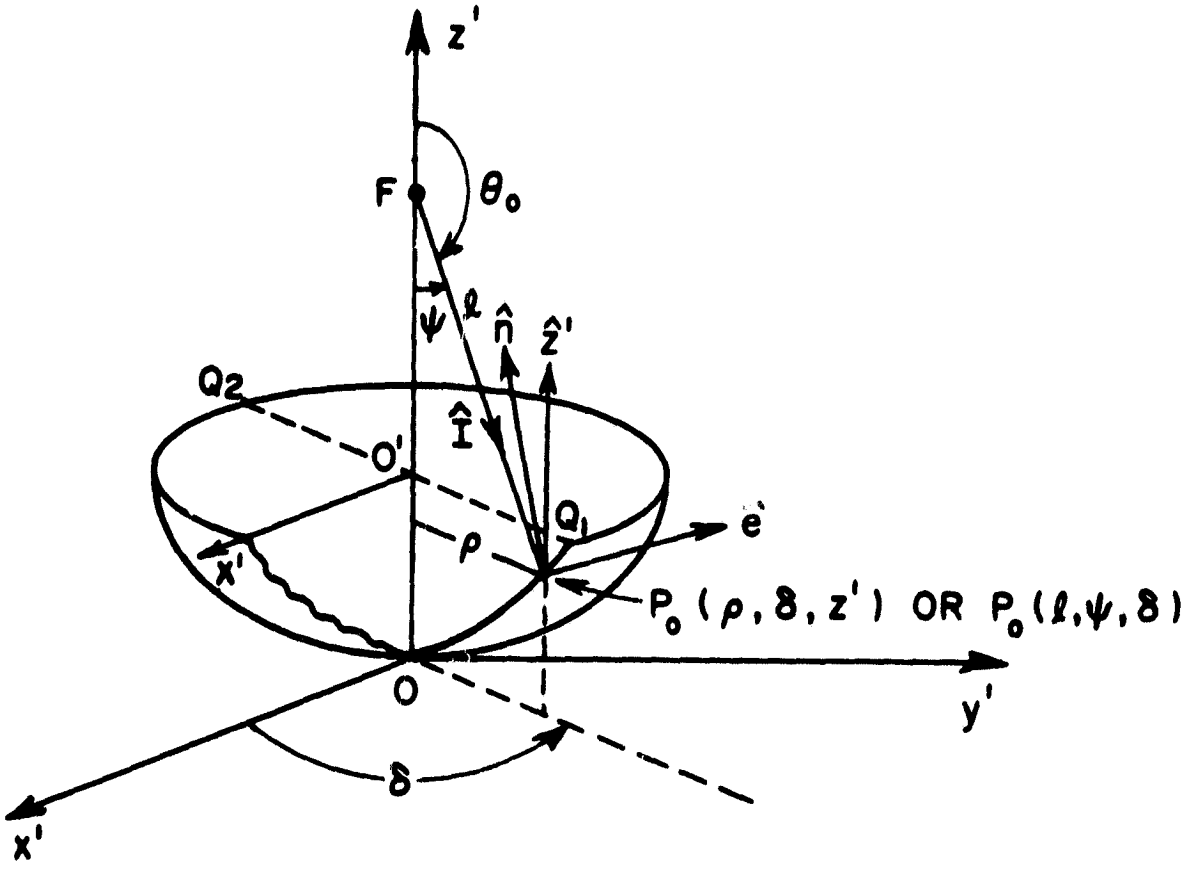

Fig. B-9.

Current Density Due to Direct Ray:

As the electric field at point P_o on the paraboloidal surface from the feed given in the form in Eq. (B-71), the corresponding magnetic field can be found as

(B-96)

$$\bar{H}^f(P_o) = \frac{1}{\eta}\hat{I} \times \bar{E}^f(P_o)$$

$$= \frac{1}{\eta}\left[\hat{e}\, Bh(\psi,\delta) - \hat{p}\, Ag(\psi,\delta)\right] \frac{e^{-jk\ell}}{\ell}$$

where $\eta = \sqrt{\frac{\mu_o}{\varepsilon_o}} = 377$ ohms is the characteristic impedance of free space. In terms of components in rectangular coordinates (x',y',z'), it becomes

(B-97)

$$\bar{H}^f(P_o) = \hat{x}' \frac{1}{\eta} [-Bh(\psi,\delta)\sin\delta + Ag(\psi,\delta)\cos\psi\cos\delta] \frac{e^{-jk\ell}}{\ell}$$

$$+ y' \frac{1}{\eta} [Bh(\psi,\delta)\cos\delta + Ag(\psi,\delta)\cos\psi\sin\delta] \frac{e^{-jk\ell}}{\ell}$$

$$+ z' \frac{1}{\eta} [Ag(\psi,\delta)\sin\psi] \frac{e^{-jk\ell}}{\ell}$$

The surface current density $\bar{K}^f(P_o)$ induced on the paraboloidal surface at point $P_o(\ell,\psi,\delta)$ due to above magnetic field then becomes

(B-98)

$$\frac{1}{2}\bar{K}^f(P_o) = \hat{n}(P_o) \times \bar{H}^f(P_o)$$

$$= \hat{x}' \frac{1}{\eta} [-Ag(\psi,\delta)\cos\frac{\psi}{2}\sin\delta - Bh(\psi,\delta)\cos\frac{\psi}{2}\cos\delta] \frac{e^{-jk\ell}}{\ell}$$

$$+ \hat{y}' \frac{1}{\eta} [-Ag(\psi,\delta)\cos\frac{\psi}{2}\cos\delta - Bh(\psi,\delta)\cos\frac{\psi}{2}\sin\delta] \frac{e^{-jk\ell}}{\ell}$$

$$+ \hat{z}' \frac{1}{\eta} [-Bh(\psi,\delta)\sin\frac{\psi}{2}] \frac{e^{-jk\ell}}{\ell}$$

Current Density Due to Edge Diffracted Ray from $Q_1(a,\delta,z_o)$:

As shown in Fig. B-9, a point $P_o(v,\xi,\delta)$ on the paraboloidal surface can also be defined as $P_o(\ell,\psi,\delta)$: it can be found that

(B-99)

$$v = \ell \sin\psi \sqrt{1 + \left(\frac{\ell \sin\psi}{4f}\right)^2}$$

$$\xi = \tan^{-1} \frac{4f}{\ell \sin\psi}$$

$$\delta = \delta$$

and

(B-100)

$$v \sin\xi = \ell \sin\psi$$

$$v \cos\xi = (\ell \sin\psi)^2/4f$$

From Eq. (B-85), the corresponding magnetic field of $\bar{E}_1^d(P_o)$ at the point $P_o(\ell,\psi,\delta)$ on the paraboloidal surface can be found as

(B-101)

$$\bar{H}_1^d(P_o) = \frac{1}{\eta}\,\hat{d}_1 \times \bar{E}_1^d(P_o)$$

$$= \frac{1}{\eta}\,[\hat{e}_1\, E_{q1}^d(P_o) - \hat{q}_1\, E_{e1}^d(P_o)]$$

$$= \hat{x}'\,\frac{1}{\eta}\left[-E_{q1}^d(P_o)\sin\delta - E_{e1}^d(P_o)\,\frac{(v\cos\xi - z_o)\cos\delta}{r_1}\right]$$

$$+ \hat{y}'\,\frac{1}{\eta}\left[E_{q1}^d(P_o)\cos\delta - E_{e1}^d(P_o)\,\frac{(v\cos\xi - z_o)\sin\delta}{r_1}\right]$$

$$+ \hat{z}'\,\frac{1}{\eta}\left[E_{e1}^d(P_o)\,\frac{v\sin\xi - a}{r_1}\right]$$

The surface current density $\bar{K}_1^d(P_o)$ induced on the paraboloidal surface at point P_o due to this magnetic field $\bar{H}_1^d(P_o)$ at that point is

(B-102)

$$\frac{1}{2}\,\bar{K}_1^d(P_o) = \hat{n}(P_o) \times \bar{H}_1^d(P_o)$$

$$= \hat{x}'\,\frac{1}{\eta}\left\{-E_{q1}^d(P_o)\cos\frac{\psi}{2}\cos\delta\right.$$

$$\left. + E_{e1}^d(P_o)\sin\delta\left[-\frac{(v\sin\xi - a)}{r_1}\sin\frac{\psi}{2} + \frac{(v\cos\xi - z_o)}{r_1}\cos\frac{\psi}{2}\right]\right\}$$

$$+ \hat{y}'\,\frac{1}{\eta}\left\{-E_{q1}^d(P_o)\cos\frac{\psi}{2}\sin\delta\right.$$

$$\left. + E_{e1}^d(P_o)\cos\delta\left[\frac{(v\sin\xi - a)}{r_1}\sin\frac{\psi}{2} - \frac{(v\cos\xi - z_o)}{r_1}\cos\frac{\psi}{2}\right]\right\}$$

$$+ z'\,\frac{1}{\eta}\left\{-E_{q1}^d(P_o)\sin\frac{\psi}{2}\right\}$$

where r_1, the distance from the edge point Q_1 to P_o, can be found as

(B-102a)
$$r_1 = \{[\ell\sin\psi\cos\delta - \ell_o\sin\Psi_o\cos\delta]^2$$
$$+ [\ell\sin\psi\sin\delta - \ell_o\sin\Psi_o\sin\delta]^2 + [\ell\cos\psi - \ell\cos\Psi_o]^2\}^{1/2}$$

Current Density Due to Edge Diffracted Ray From $Q_2(a,\pi+\delta,z_o)$:

From Eq. (B-91), the corresponding magnetic field of $\bar{E}_2^d(P_o)$ at the point $P_o(\ell,\psi,\delta)$ on the paraboloidal surface can be found through

(B-103)

$$\overline{H}_2^d(P_o) = \hat{n}(P_o) \times \overline{E}_2^d(P_o)$$

$$= \frac{1}{\eta}\left[\hat{e}_2\, E_{q2}^d(P_o) - \hat{q}_2\, E_{q2}^d(P_o)\right]$$

$$= \hat{x}'\,\frac{1}{\eta}\left[E_{q2}^d(P_o)\sin\delta + E_{e2}^d(P_o)\,\frac{(v\cos\xi - z_o)\cos\delta}{r_2}\right]$$

$$+ \hat{y}'\,\frac{1}{\eta}\left[-E_{q2}^d(P_o)\cos\delta + E_{e2}^d(P_o)\,\frac{(v\cos\xi - z_o)\sin\delta}{r_2}\right]$$

$$+ \hat{z}'\,\frac{1}{\eta}\left[-E_{e2}^d(P_o)\,\frac{(v\sin\xi + a)}{r_2}\right]$$

The surface current density induced on the paraboloidal surface at the point $P_o(\ell,\psi,\delta)$ due to this magnetic field is then

(B-104)

$$\frac{1}{2}\,\overline{K}_2^d(P_o) = \hat{n}(P_o) \times \overline{H}_2^d(P_o)$$

$$= \hat{x}'\,\frac{1}{\eta}\left\{E_{q2}^d(P_o)\cos\frac{\psi}{2}\cos\delta\right.$$

$$\left. + E_{e2}^d(P_o)\sin\delta\left[\frac{(v\sin\xi + a)}{r_2}\sin\frac{\psi}{2} - \frac{(v\cos\xi - z_o)}{r_2}\cos\frac{\psi}{2}\right]\right\}$$

$$+ \hat{y}'\,\frac{1}{\eta}\left\{-E_{q2}^d(P_o)\cos\frac{\psi}{2}\sin\delta\right.$$

$$\left. + E_{e2}^d(P_o)\cos\delta\left[\frac{-(v\sin\xi + a)}{r_2}\sin\frac{\psi}{2} - \frac{(v\cos\xi - z_o)}{r_2}\cos\frac{\psi}{2}\right]\right\}$$

$$+ \hat{z}'\,\frac{1}{\eta}\left\{E_{q2}^d(P_o)\sin\frac{\psi}{2}\right\}$$

where r_2, the distance from the edge point Q_2 to P_o, can be obtained as

(B-104a) $$r_2 = \{[\ell\sin\psi\cos\delta - \ell_o\sin\Psi_o\cos(\pi+\delta)]^2$$

$$+ [\ell\sin\psi\sin\delta - \ell_o\sin\Psi_o\sin(\pi+\delta)]^2 + [\ell\cos\psi - \ell_o\cos\Psi_o]^2\}^{1/2}$$

The current density due to both edge diffracted rays is the sum of the contributions of $\overline{K}_1^d(P_o)$ and $\overline{K}_2^d(P_o)$. Let the sum be denoted by $\overline{K}_s^d(P_o)$ where the subscript "s" stands for the contribution from the circular edge of its own reflector where the point P_o is considered.

(B-105)

$$\frac{1}{2}\bar{K}_s^d(P_o) = \hat{x}'\,\frac{1}{\eta}\left\{\left[-E_{q1}^d(P_o) + E_{q2}^d(P_o)\right]\cos\frac{\psi}{2}\cos\delta\right.$$
$$+\left[-E_{e1}^d(P_o)\,\frac{(v\sin\xi - a)}{r_1} + E_{e2}^d(P_o)\,\frac{v\sin\xi + a}{r_2}\right]\sin\frac{\psi}{2}\sin\delta$$
$$\left.+\left[\frac{E_{e1}^d(P_o)}{r_1} - \frac{E_{e2}^d(P_o)}{r_2}\right](v\cos\xi - z_o)\cos\frac{\psi}{2}\sin\delta\right\}$$
$$+\hat{y}'\,\frac{1}{\eta}\left\{-\left[E_{q1}^d(P_o) + E_{q2}^d(P_o)\right]\cos\frac{\psi}{2}\sin\delta\right.$$
$$+\left[E_{e1}^d(P_o)\,\frac{(v\sin\xi - a)}{r_1} - E_{e2}^d(P_o)\,\frac{(v\sin\xi + a)}{r_2}\right]\sin\frac{\psi}{2}\cos\delta$$
$$\left.+\left[-\frac{E_{e1}^d(P_o)}{r_1} - \frac{E_{e2}^d(P_o)}{r_2}\right](v\cos\xi - z_o)\cos\frac{\psi}{2}\cos\delta\right\}$$
$$+\hat{z}'\,\frac{1}{\eta}\left[-E_{q1}^d(P_o) + E_{q2}^d(P_o)\right]\sin\frac{\psi}{2}$$

where η is the characteristic impedance of free space; the components of the diffracted field, $E_{e1}^d(P_o)$, $E_{q1}^d(P_o)$, $E_{e2}^d(P_o)$, and $E_{q2}^d(P_2)$, are given in Eqs. (B-85a), (B-85b), (B-92a), and (B-92b) respectively. The parameters in the above equations are also given in Eqs. (B-85) and (B-92) respectively. It is noted that the region under consideration is the one bounded by the parabolic reflector and its aperture; in this region the coordinates of point $P_o(v,\xi,\delta)$ on the paraboloidal surface are given in Eq. (B-99), and the difference and sum of the diffracted and incident angles, $\beta_d(Q_i)$ and $\beta_i(Q_i)$, for both edge points are given in Table B-2 as the formulation for Region 1.

(d) Surface Current Contribution on a Parabolic Reflector Through Edge Diffraction Mechanism from Adjacent Parabolic Reflector in a Closely Spaced Array

A two-element array of parabolic reflector antennas with their axes pointing in (θ',ϕ') direction is shown in Figs. B-10,11. The first parabolic reflector antenna is located with its vertex at the origin O of the fixed rectangular coordinate (x,y,z). The second parabolic reflector antenna is located with its vertex at point A along y-axis a distance "d" away from the origin O. For the scanning performed in the yz-plane, a portion of the edge diffracted rays originated from edge points T_1 and T_2 on the circular edge of the second paraboloid is collected by the first paraboloid. These edge diffracted rays collected by the first paraboloid introduce a secondary current density, on the first paraboloidal surface, which becomes the second correction factor to the primary current density induced by the direct ray from

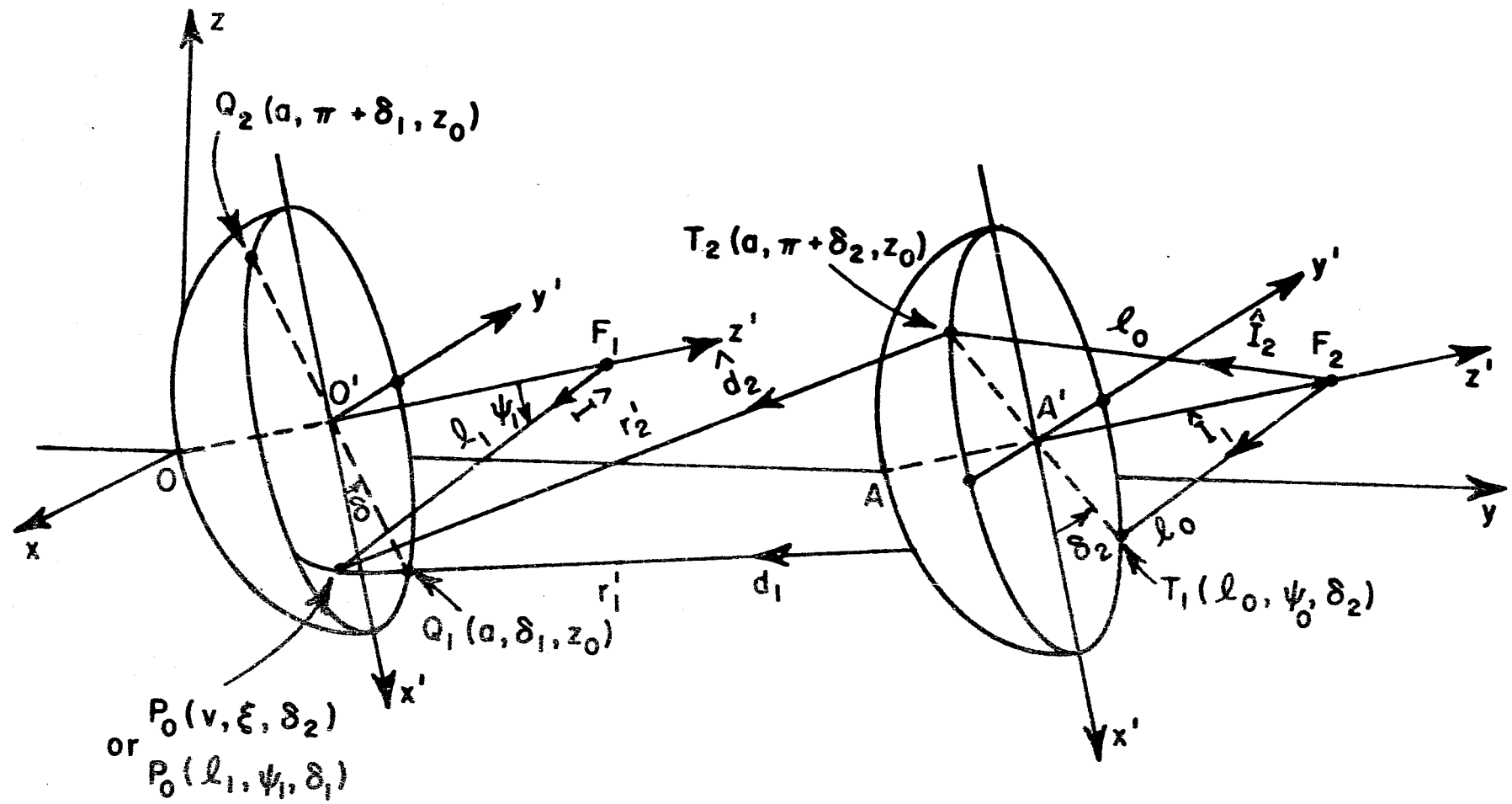
z
$Q_2(a, \pi+\delta_1, z_0)$
$T_2(a, \pi+\delta_2, z_0)$
y'
z'
F_1
d_2
ℓ_1 ψ_1
r_2'
O'
O
r_0
x
A'
A
ℓ_0
$\hat{I}_2$
F_2
$\hat{I}_1$
y
δ_2
ℓ_0
$T_1(\ell_0, \psi_0, \delta_2)$
r_1'
d_1
$Q_1(a, \delta_1, z_0)$
x'
$P_0(v, \xi, \delta_2)$
or
$P_0(\ell_1, \psi_1, \delta_1)$

Fig. B-10.

its feed antenna in addition to the first correction factor discussed in Sec. 3c. Consequently the mutual coupling and the blocking effect may be investigated.

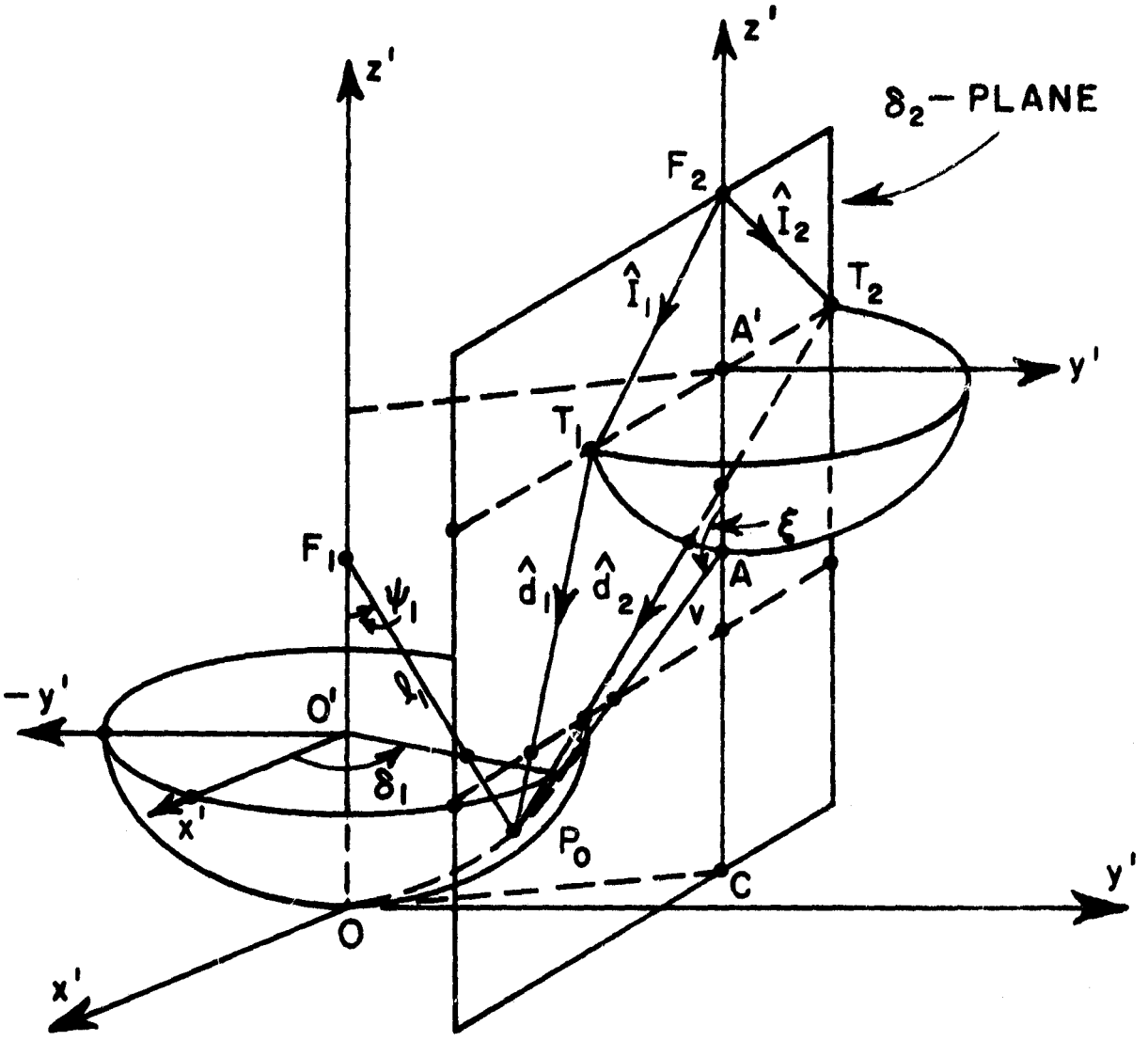

Fig. B-11.

A point $P_o(\ell_1,\psi_1,\delta_1)$ on the first paraboloid is also defined by (v,ξ,δ_2) in the spherical coordinate with its origin at point A where v is the distance from point A to point P_o; ξ is the polar angle measured from the z'-axis of the second paraboloid; δ_2 is the azimuth angle measured from x'-axis of the second paraboloid. A point on the second paraboloidal surface is defined by (ℓ_2,ψ_2,δ_2).

The edge diffracted field, originated both from edge points $T_1(\ell_o,\psi_o,\delta_2)$ and $T_2(\ell_o,\psi_o,\pi+\delta_2)$ on the second parabolic reflector, at point $P_o(v,\xi,\delta_2)$ on the first paraboloid is given in Eq. (B-93). In the analysis to follow, it is assumed that the point $P_o(\ell_1,\psi_1,\delta_1)$ is visible from both edge points, T_1 and T_2, on the second paraboloid, hence

(B-106) $$\overline{E}^d(P_o) = \overline{E}_1^d(P_o) + \overline{E}_2^d(P_o)$$

For the case that one edge point is not visible from the point $P_o(\ell_1,\psi_1,\delta_1)$ then the diffracted field originated from that point is simply zero. The fields $\overline{E}_1^d(P_o)$ and $\overline{E}_2^d(P_o)$ are the edge diffracted fields originated from edge point T_1 and T_2 respectively. They are given in Eqs. (B-85) and (B-92) respectively. The magnetic fields associated with $\overline{E}_1^d(P_o)$ and $\overline{E}_2^d(P_o)$ generated by the second parabolic reflector are given in Eqs. (101) and (103). For the reason to avoid confusion, they are repeated below as

(B-107)

$$\overline{H}_1^d(P_o) = \hat{x}'\,\frac{1}{\eta}\left[-E_{q1}^d(P_o)\sin\delta_2 - E_{e1}^d(P_o)\,\frac{(v\cos\xi - z_o)\cos\delta_2}{r_1'}\right] + \hat{y}'\,\frac{1}{\eta}\left[E_{q1}^d(P_o)\cos\delta_2 - E_{e1}^d(P_o)\,\frac{(v\cos\xi - z_o)\sin\delta_2}{r_1'}\right] + \hat{z}'\,\frac{1}{\eta}\left[E_{e1}^d(P_o)\,\frac{(v\sin\xi - a)}{r_1'}\right]$$

(B-108)

$$\overline{H}_2^d(P_o) = \hat{x}'\,\frac{1}{\eta}\left[E_{q2}^d(P_o)\sin\delta_2 + E_{e2}^d(P_o)\,\frac{(v\cos\xi - z_o)\cos\delta_2}{r_2'}\right] + \hat{y}'\,\frac{1}{\eta}\left[-E_{q2}^d(P_o)\cos\delta_2 + E_{e2}^d(P_o)\,\frac{(v\cos\xi - z_o)\sin\delta_2}{r_2'}\right] + \hat{z}'\,\frac{1}{\eta}\left[-E_{e2}^d(P_o)\,\frac{v\sin\xi + a}{r_2'}\right]$$

The magnetic field at the point $P_o(\ell_1,\psi_1,\delta_1)$ on the first paraboloid due to the edge diffraction generated from the second paraboloid is denoted $\overline{H}_m^d(P_o)$ where the subscript "m" and the superscript "d" stand for the contribution from the adjacent reflector through edge diffraction mechanism. Hence, $\overline{H}_m^d(P_o)$ is the sum of $\overline{H}_1^d(P_o)$ and $\overline{H}_2^d(P_o)$ given in Eqs. (B-107) and (B-108) respectively, it is given as

(B-109)

$$\overline{H}_m^d(P_o) = \hat{x}'\,\frac{1}{\eta}\left\{\left[-E_{q1}^d(P_o) + E_{q2}^d(P_o)\right]\sin\delta_2 - E_{e1}^d(P_o)\,\frac{(v\cos\xi - z_o)\cos\delta_2}{r_1'} + E_{e2}^d(P_o)\,\frac{(v\cos\xi - z_o)\cos\delta_2}{r_2'}\right\} + y'\,\frac{1}{\eta}\left\{\left[E_{q1}^d(P_o) - E_{q2}^d(P_o)\right]\cos\delta_2 - E_{e1}^d(P_o)\,\frac{(v\cos\xi - z_o)\sin\delta_2}{r_1'} + E_{e2}^d(P_o)\,\frac{(v\cos\xi - z_o)\sin\delta_2}{r_2'}\right\} + \hat{z}'\,\frac{1}{\eta}\left\{E_{e1}^d(P_o)\,\frac{v\sin\xi - a}{r_1'} - E_{e2}^d(P_o)\,\frac{v\sin\xi + a}{r_2'}\right\}$$

where, from Eq. (85) and Eq. (92)

(B-110a)

$$E^d_{e_{q1}}(P_o) = E^f_{e_p}(T_1) \cdot \frac{-e^{-j\frac{\pi}{4}}}{2\sqrt{2\pi k}} \cdot \left[\frac{F(kL_1 a_-(T_1))}{\cos\frac{\beta_d(T_1)-\beta_i(T_1)}{2}} \mp \frac{F(kL_1 a_+(T_1))}{\cos\frac{\beta_d(T_1)-\beta_i(T_1)}{2}} \right] \cdot \frac{1}{\sqrt{r'_1}} \sqrt{\frac{a}{v \sin\xi}}\, e^{-jkr'_1}$$

(110b)

$$E^d_{e_{q2}}(P_o) = E^f_{e_p}(T_2) \cdot \frac{-e^{-j\frac{\pi}{4}}}{2\sqrt{2\pi k}} \cdot \left[\frac{F(kL_2 a_-(T_2))}{\cos\frac{\beta_d(T_2)-\beta_i(T_2)}{2}} \mp \frac{F(kL_2 a_+(T_2))}{\cos\frac{\beta_d(T_2)-\beta_i(T_2)}{2}} \right] \cdot \frac{j}{\sqrt{r'_2}} \sqrt{\frac{a}{v \sin\xi}}\, e^{-jkr'_2}$$

with

(B-110c) $E^f_e(T_1) = Ag(\Psi_o, \delta_2) \frac{e^{-jk\ell_o}}{\ell_o}$

(B-110d) $E^f_p(T_1) = Bh(\Psi_o, \delta_2) \frac{e^{-jk\ell_o}}{\ell_o}$

(B-110e) $E^f_e(T_2) = Ag(\Psi_o, \pi+\delta_2) \frac{e^{-jk\ell_o}}{\ell_o}$

(B-110f) $E^f_p(T_2) = Bh(\Psi_o, \pi+\delta_2) \frac{e^{-jk\ell_o}}{\ell_o}$

(B-110g) $a_\mp(T_i) = 1 + \cos[\beta_d(T_i) \mp \beta_i(T_i)]$, $i = 1,2$

(B-110h) $$L_i = \frac{r_i' \ell_o}{r_i' + \ell_o}, \quad i = 1,2$$

(B-110i)

$$F(kL_i a_{\mp}(T_i)) = j2\sqrt{kL_i a_{\mp}(T_i)}\; e^{jkL_i a_{\mp}(T_i)} \cdot \int_{\sqrt{kL_i a_{\mp}(T_i)}}^{\infty} e^{-j\tau^2}\, d\tau$$

Since the first parabolic reflector is behind the second one when scanning is performed in yz-plane as shown in Figs. B-10,11, the region under consideration is the space behind the aperture plane of the second reflector. The difference and sum of $\beta_d(T_i)$ and $\beta_i(T_i)$ are the values given in Regions 4 and 5 in Table B-2 for both $i = 1,2$. The values on the boundaries are given in Table B-3.

This magnetic field $\overline{H}_m^d(P_o)$ at point $P_o(\ell_1,\psi_1,\delta_1)$ on the first paraboloid induces a surface current density $\overline{K}_m^d(P_o)$, at that particular point, which becomes the second correction factor to the primary current density induced by the direct ray at point P_o from the feed in addition to the first correction factor $\overline{K}_s^d(P_o)$ given in Eq. (B-105); $\overline{K}_m^d(P_o)$ can be found by

(B-111) $$\frac{1}{2}\ \overline{K}_m^d(P_o) = \hat{n}(P_o) \times \overline{H}_m^d(P_o)$$

where $\hat{n}(P_o)$ is the unit vector normal to the first paraboloidal surface at point $P_o(\ell_1,\psi_1,\delta_1)$; it is given as

(B-112) $$\hat{n}(P_o) = \hat{x}'(-\sin\ \frac{\psi_1}{2}\cos\ \delta_1) + \hat{y}'\ (-\sin\ \frac{\psi_1}{2}\sin\ \delta_1) + \hat{z}'\cos\ \frac{\psi_1}{2}$$

Substituting Eqs. (B-109) and (B-112) into (B-111), $\overline{K}_m^d(P_o)$ becomes

(B-113)

$$\frac{1}{2}\overline{K}_m^d(P_o) = \hat{x}'\,\frac{1}{\eta}\left\{\left[-E_{q1}^d(P_o) + E_{q2}^d(P_o)\right]\cos\frac{\psi_1}{2}\cos\delta_2 + \left[-\frac{E_{e1}^d(P_o)}{r_1'}(v\sin\xi - a) + \frac{E_{e2}^d(P_o)}{r_2'}(v\sin\xi + a)\right]\cdot \sin\frac{\psi_1}{2}\sin\delta_1 + \left[\frac{E_{e1}^d(P_o)}{r_1'} - \frac{E_{e2}^d(P_o)}{r_2'}\right](v\cos\xi - z_o)\cos\frac{\psi_1}{2}\sin\delta_2\right\}$$

$$+ \hat{y}'\,\frac{1}{\eta}\left\{\left[-E_{q1}^d(P_o) + E_{q2}^d(P_o)\right]\cos\frac{\psi_1}{2}\sin\delta_2 + \left[\frac{E_{e1}^d(P_o)}{r_1'}(v\sin\xi - a) - \frac{E_{e2}^d(P_o)}{r_2'}(v\sin\xi + a)\right]\sin\frac{\psi_1}{2}\cos\delta_1 + \left[-\frac{E_{e1}^d(P_o)}{r_1'} + \frac{E_{e2}^d(P_o)}{r_2'}\right](v\cos\xi - z_o)\cos\frac{\psi_1}{2}\cos\delta_2\right\}$$

$$+ \hat{z}'\,\frac{1}{\eta}\left\{\left[-E_{q1}^d(P_o) + E_{q2}^d(P_o)\right]\sin\frac{\psi_1}{2}\cos(\delta_1-\delta_2) + \left[-\frac{E_{e1}^d(P_o)}{r_1'} + \frac{E_{e2}^d(P_o)}{r_2'}\right]\sin\frac{\psi_1}{2}\sin(\delta_1-\delta_2)\right\}$$

(e) Summary

With a two-element array of parabolic reflector antennas as arranged in Fig. B-10, the total induced surface current density at a point $P_o(\ell_1,\psi_1,\delta_1)$ on the first parabolic reflector is the sum of the contributions of the direct ray from its feed antenna, two singly edge-diffracted rays originated from edge points $Q_1(a,\delta,z_o)$ and $Q_2(a,\pi+\delta,z_o)$ on the same parabolic reflector where $P_o(\ell_1,\psi_1,\delta_1)$ is located, and two singly edge-diffracted rays, originated from edge points $T_1(a,\delta_2,z_o)$ and $T_2(a,\pi+\delta_2,z_o)$ on the second parabolic reflector, incident on point $P_o(\ell_1,\psi_1,\delta_1)$. Thus, the total induced surface current density $\overline{K}(P_o)$ at point $P_o(\ell_1,\psi_1,\delta_1)$ on the first parabolic reflector becomes

(B-114) $$\overline{K}(P_o) = \overline{K}^f(P_o) + \overline{K}_s^d(P_o) + \overline{K}_m^d(P_o)$$

where

$\overline{K}^f(P_o)$ is the current density induced by the direct ray from the feed of the first parabolic reflector; it is given in Eq. (98),

$\overline{K}_s^d(P_o)$ is the current density induced by two singly edge-diffracted rays from edge points Q_1 and Q_2 on the first parabolic reflector as formulated in Eq. (105),

$\overline{K}_m^d(P_o)$ is the current density induced by two singly edge-diffracted rays from edge points T_1 and T_2 on the second parabolic reflector as given in Eq. (B-113).

The total surface current density $\overline{KK}(Q_o)$ at a point $Q_o(\ell_2,\psi_2,\delta_2)$ on the second parabolic reflector is the sum of the contributions of the direct ray from the feed on the second parabolic reflector and two singly edge-diffracted rays from edge points T_1 and T_2 on the second parabolic reflector. Thus,

$$\text{(B-115)} \quad \overline{KK}(Q_o) = \overline{KK}^f(Q_o) + \overline{KK}_s^d(Q_o)$$

where $\overline{KK}^f(Q_o)$ and $\overline{KK}_s^d(Q_o)$ are given in Eqs. (B-98) and (B-105) respectively with ψ, δ, and ℓ replaced respectively by ψ_2, δ_2, and ℓ_2 for the second paraboloid in the array.

The electric and magnetic fields in the far-zone region of a single paraboloid can be obtained by an integration of the surface current density over the reflector surface. The fields in the far-zone region of an array of parabolic reflector antennas are the linear sum of contributions from each paraboloid in the array. The fields for a single paraboloid are given as (Ref. B-11)

$$\overline{E}(R,\theta,\phi) = -\frac{j\omega\mu}{2\pi}\frac{e^{-jkR}}{R}\int_A \left[\frac{\overline{K}}{2} - \left(\frac{\overline{K}}{2}\cdot\hat{R}\right)\hat{R}\right] e^{-jk\overline{\rho}\cdot\hat{R}}\, dS$$

$$\overline{H}(R,\theta,\phi) = \frac{1}{\eta}\left[\hat{R} \times \overline{E}(R,\theta,\phi)\right]$$

where R is the distance from the origin to the observation point and $\hat{R}$ is a unit vector in that direction; $\hat{\rho}$ is the distance from the origin to the element of surface and $\overline{\rho} = \rho\hat{\rho}$ with $\hat{\rho}$ being the unit vector in that direction; $\overline{K}$ is the surface current density on the surface.

The formulations in this section employ the current distribution method. The radiation pattern of the array can also be obtained by employing aperture distribution method. In aperture distribution method, there are two correction factors which arise from the edge diffraction mechanism in addition to the distribution of the direct ray from the

feed through single reflection on the concave surface of a paraboloid; one is the aperture distribution of the singly edge-diffracted rays from edge points of the reflector where the field is observed and the other one is the aperture distribution due to the singly edge-diffracted rays from edge points on the adjacent reflector. Both the current and aperture distribution methods predict successfully the radiation pattern of a parabolic reflector in the forward axial region (Ref. B-12). It will not, however, give an accurate wide angle radiation pattern especially in the backlobe region. It is known that an accurate noise temperature of the overall system depends upon the accuracy of the radiation pattern of the overall system. To obtain wide angle radiation pattern of the system, one vital type of ray must be considered in addition to the three types of rays mentioned above. The fourth ray is the reflected ray by the convex surface of a reflector. The most difficult task in the ray tracing technique in a three dimensional problem, such as this one, is to find the boundaries of regions where each single type of ray is valid.

There are no numerical calculations obtained for Eqs. (B-114) and (B-115) at this time. The results will be included in the future report.

The preparation for an experimental array of two dishes has been initiated. One 2-foot sharp edge parabolic reflector which has been ordered with another identical one which this Laboratory owns will be used to form the array. The feed of the reflector will be an open ended flanged rectangular waveguide. The feed support will consist of a tripod which is fabricated of polystyrene. The outdoor supporting structure for the array is in progress.

The following steps are going to be taken in the course of this study:

1) A continuing effort will be devoted to the theoretical study of this problem. The current-distribution and aperture-distribution methods, and the geometrical theory of diffraction will be applied to solve the proposed problem.

2) A comparison between the results obtained by using different methods will be made in order to observe any discrepency and hopefully it may be interpreted.

3) During the above investigations, it may be necessary to look into the possibility to apply a combination of the aforementioned methods at different stages along the course of solving the proposed problem in order to obtain better results.

4) While the theoretical study is being performed, an experimental array of two dishes with a diameter of a few feet will be designed and tested in S-band (or in X-band depending upon the availability of equipment) in order to compare the measured data with theoretical results predicted by the above methods.

5) An experimental array of more elements, four or six dishes (again, depending upon the availability of equipment) may be tested in order to observe any unusual behaviors which are not predictable by a two-dish array.

REFERENCES

B-1. Private Communication of work done by the Andrews Corporation, Chicago, Illinois for the Collins Radio Corporation.

B-2. Private Communication from J. Reiche, Hughes Aircraft Company, Culver City, California as an Interdepartmental Correspondence.

B-3. Keller, J.B., "Diffraction by an Aperture," J. Appl. Phys., Vol. 28, No. 6, pp. 426-444, April 1957.

B-4. Keller, J.B., "The Geometrical Theory of Diffraction," J. Opt. Soc. Am., vol. 52, pp. 116-130, February 1962.

Rudduck, R.C. and Tsai, L.L., "Aperture Reflection Coefficient of a Parallel-Plate Waveguide by Wedge Diffraction Analysis," Report 1691-20, April 10, 1966, ElectroScience Laboratory, The Ohio State University Research Foundation; prepared under Grant NsG-448, NASA, Washington, D.C.

Tsai, L.L., Rudduck, R.C., and Dybdal, R.B., "Coupling Between Parallel-Plate Waveguides by Wedge Diffraction Techniques," Report 1691-17, October 20, 1965, ElectroScience Laboratory, The Ohio State University Research Foundation; prepared under Grant NsG-448, NASA, Washington, D.C.

Ryan, C.E., Jr., Rudduck, R.C., "A Wedge Diffraction Analysis of the Radiation Patterns of Parallel-Plate Waveguide," IEEE Trans. Antennas and Propagation, AP-16, No. 4, pp. 490-1, July 1968.

Rudduck, R.C. and Tsai, L.L., "Aperture Reflection Coefficient of TEM and TE_{01} Mode Parallel-Plate Waveguides," IEEE Trans. Antennas and Propagation, vol. AP-16, pp. 83-89, January 1968.

Dybdal, R.B., Rudduck, R.C., and Tsai, L.L., "Mutual Coupling Between TEM and TE_{01} Parallel-Plate Waveguide Apertures," IEEE Trans. Antennas and Propagation, AP-14, No. 5, September 1966, pp. 574-580.

B-5. Rusch, W.V.T., "Edge Diffraction from Truncated Paraboloids and Hyperboloids," Jet Propulsion Laboratory Technical Report 32-1113, California Institute of Technology, Pasadena, California, June 1967.

B-6. Ratnasiri, P.A.J., Kouyoumjian, R.G. and Pathak, P.H., "The Wide Angle Side Lobes of Reflector Antennas," Report 2183-1, 23 March 1970, ElectroScience Laboratory, Department of Electrical Engineering, The Ohio State University; prepared under Contract AF 19(628)-5929 for Electronic Systems Division, Air Force Systems Command.

B-7. Keller, J.B., "Diffraction by a Convex Cylinder," IRE Transactions on Antennas and Propagation, Vol. AP-4, No. 3, pp. 312-321, July 1956.

B-8. Keller, J.B. and Levy, B., "Diffraction by a Smooth Object," Commun. Pure Appl. Math., vol. 12, pp. 159-209, 1959.

B-9. Keller, Lewis, and Seckler, "Asymptotic Solution of Some Diffraction Problems," Commun. Pure Appl. Math., Vol. 9, 1956.

B-10. Kouyoumjian, R.G., "Asymptotic High Frequency Methods," Proc. of the IEEE, Vol. 53, pp. 864-876, 1965.

B-11. Silver, S., Microwave Antenna Theory and Design, BTP, Inc., 1964, p. 149.

B-12. Silver, op cit., Chapter 12, p. 415.

C. A PHASED ARRAY OF SMALL CLOSELY SPACED ELEMENTS ORGANIZED INTO SUB-APERTURES - ELECTRONICALLY STEERABLE
(See Status Report Number 4, 15 February 1970, Grant Number NGR-17-004-013)

D. A SELF STEERING ARRAY - ADAPTIVE SYSTEM STUDIES
(See Technical Report 2902-1, July 1970 on Grant NGL 36-008-138 by Robert L. Riegler).

V. PLANS FOR FUTURE ACTIVITIES

This program has now or will shortly complete the assigned tasks and studies that have been outlined in Section II of this report. This means that an assessment of the virtues of one type of large ground-based antennas over another for a specific application and within the available technology can be easily accomplished to achieve the basic objectives of this program as described in Section I. Thus, future attention in this program will be turned to the problems concerning the antennas on the spacecraft itself and methods for analyzing their performance characteristics on complex structures.

The Application of Integral Equation Techniques to the Evaluation of Spacecraft Antenna Parameters

When one or more antennas are mounted on an aircraft, satellite, space shuttle, or other vehicle, their performance characteristic in terms of vehicle configuration, antenna orientation, and mutual interaction is of primary interest to the basic communication system design. Thus, the patterns and impedances, and the coupling between each pair of antennas must be carefully and accurately evaluated. These parameters may be analyzed using the geometrical theory of diffraction (GTD) at high frequencies where the antenna and its environment may be many wavelengths in extent. However at low frequencies where the antenna or the vehicle itself is small in terms of wavelength, other types of mathematical representations can be successfully applied to describe with good agreement the behavior of antennas on odd shaped vehicles or those involving complex interactions among themselves or with a ground plane. The need for both approaches is emphasized when consideration is being given to space shuttles which will be as large as the Boeing-747 aircraft and where antennas are contemplated operating with frequency ranges located appropriately from 40 MHz to K_a-band. Thus, many diverse antenna types such as slots or arrays of slots and other flush mounted antennas appropriate to a particular application are to be examined in an effort to develop methods for analyzing viable structures. Antenna evaluation for complex vehicles has traditionally been achieved by means of experimental models. This costly and time consuming approach should be supplemented by computer analyses, particularly in the design state.

At low frequencies it is convenient to formulate the radiation problem as an integral equation. By suitable finite expansion of the unknown function (such as the current density on the surface of the vehicle), the integral equation is reduced to a system of simultaneous linear equations by enforcing the boundary conditions at discrete points. We have solved numerous problems in using this point-matching technique as illustrated by the following examples.

1. Scattering by dielectric cylinders[1]
2. Arbitrary array of thin wires[2]
3. Scattering by conducting targets with arbitrary shape[3]
4. Dipole antenna on conducting cone,[4] sphere[5] or cylinder[5]
5. Dipole and loop antennas on aircraft[6]

In 1969, Richmond used Rumsey's reaction concept to develop a stationary solution for a wide class of wire antennas and scatterers. In contrast with the point-matching method, the reaction technique has no lower limit on the wire radius. For a straight or curved wire with a length of one wavelength, our reaction approach yields a system of ten or less simultaneous linear equations, whereas the point-matching method requires 32 to 100 equations. We have applied this new technique to the analysis of numerous problems concerning wire antennas. Several examples are listed below:

1. V-antenna array on NASA satellite[7]
2. Three-dimensional dipoles[8] and loop antennas[9]
3. Scattering by wire tripods and quadripods[10]
4. Yagi array of V-dipoles[11]
5. Array of TEM-line antennas[12,13]
6. Adaptive array[14]

In addition, the technique is currently being employed in the analysis and design of arrays for short-pulse transmission and reception.

The reaction technique is not limited to thin-wire problems. It readily yields the solution for scattering by conducting cylinders that are not figures of revolution (two-dimensional). For example, Fig. 1 shows the calculated results for backscattering by a square cylinder. The calculated current distributions agree with data published by Mei and Van Bladel. Figure 2 shows the calculated pattern of a half-wave slot antenna on a square cylinder.

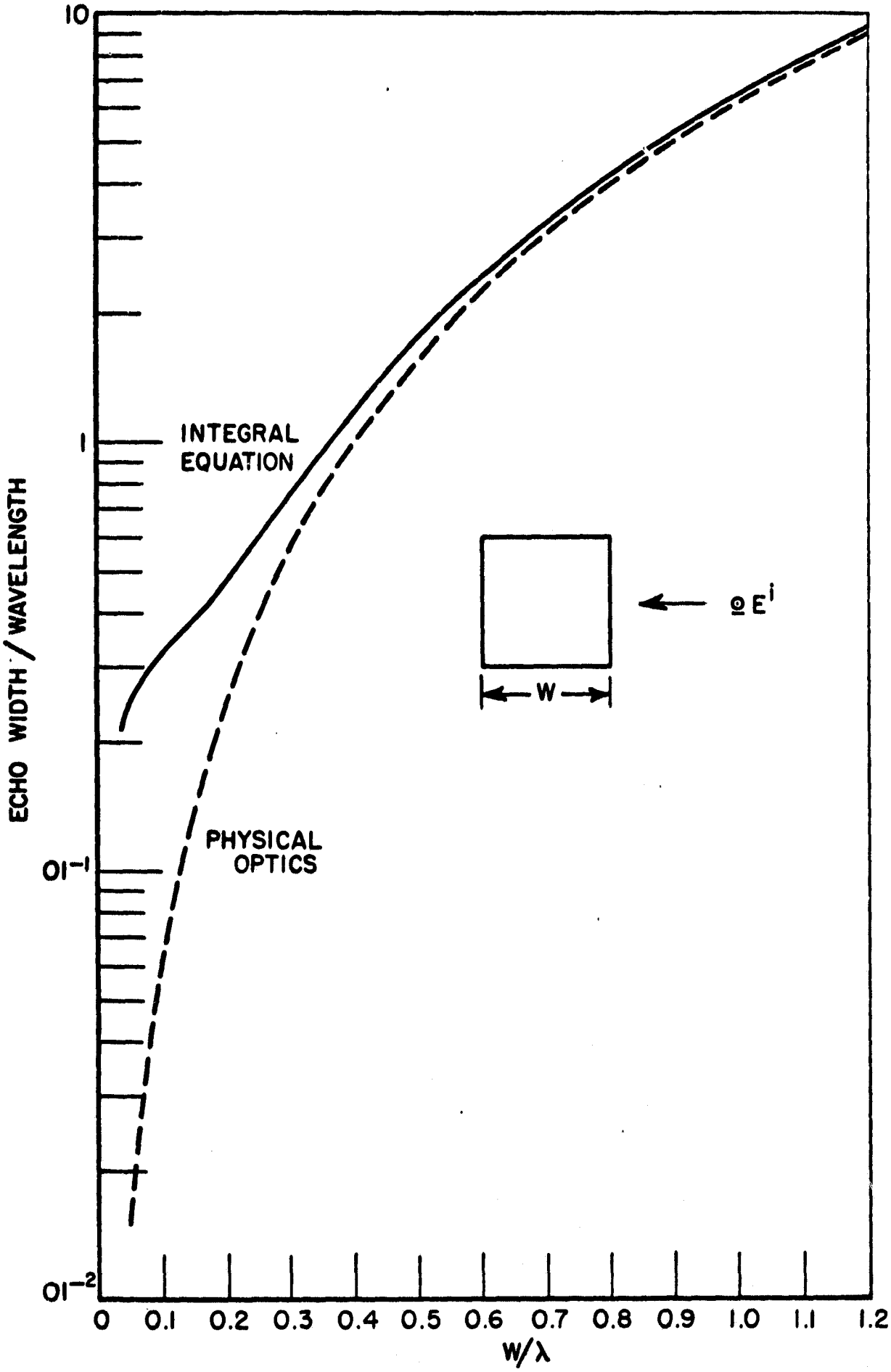

Fig. 1. Backscattering by square cylinder, normal incidence, TM case.

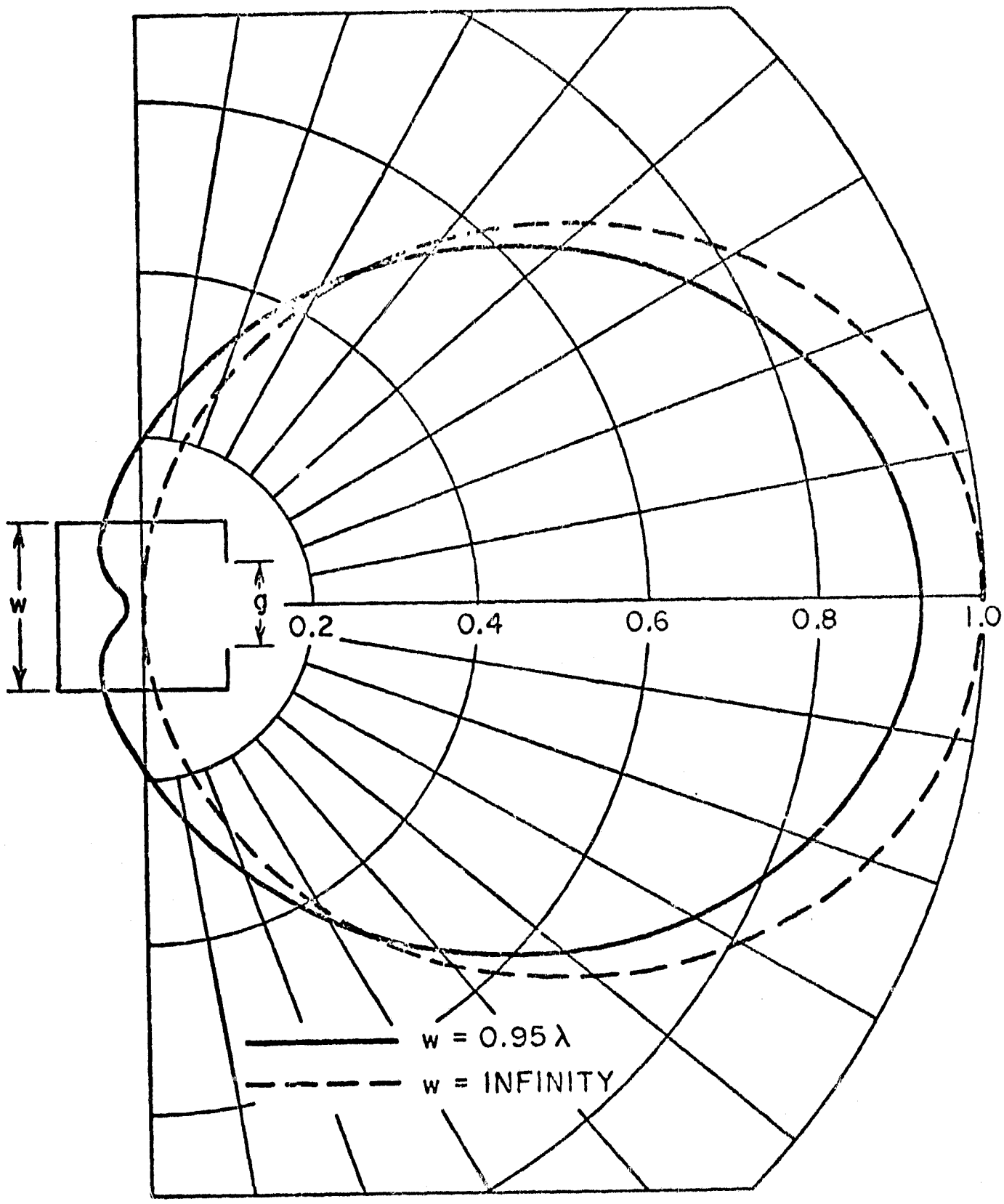

Fig. 2. Field patterns of half-wave slot antenna in square cylinder, TM case. $E_z(\phi)$ versus ϕ.
Slot width: $g = 0.5\lambda$
Aperture distribution: $E_z = \cos ky$.

Our solution proceeds as follows. We set up an array of "test sources" in the interior of the conducting body and force the unknown surface current to have the correct reaction with each test source. This yields the system of simultaneous linear equations. By locating the test sources in the interior region, some distance away from the surface, we avoid difficult and expensive integrations. With the square cylinder, for example, we placed the test sources on an interior square cylinder with width w'. The results were found to be insensitive to the size of the testing surface. The calculated echo-width was identical for w'/w = 0.5, 0.6, 0.7, 0.8 and 0.9, where w represents the half-width of the conducting cylinder.

Although we have not yet applied the reaction technique to three-dimensional problems, the advantages are already apparent. First, this technique yields a stationary solution. Second, the technique is versatile and easily programmed for digital computations. Finally, it leads to nonsingular integrals that are readily evaluated. This effort will supplement the antenna evaluation using high frequency being pursued at NASA and other existing programs at OSU. We propose to employ low-frequency techniques when the vehicle is small, a hybrid solution when the antenna is small but the vehicle is large, and high frequency techniques when both the antenna and the space shuttle craft are large in terms of wavelength.

Proposed New Work Statement

In keeping with the basic objectives of this program, the ElectroScience Laboratory of the Ohio State University proposes that a new phase of the effort be started to assist in the design of antennas on complex vehicle structures appropriate to the space shuttle operation between the earth and an orbiting satellite. Here we propose to develop computerized solutions for antenna elements mounted on odd shaped three-dimensional bodies which might be portions of an aircraft, a satellite or space shuttle vehicle. The characteristics to be obtained in an effort to provide useful design data are the three dimensional patterns and the impedance matrix which includes the various self and mutual impedances involved in the interactions amongst the antennas themselves and with their complex ground planes. This effort is to concern itself with integral equation techniques to evaluate the various pertinent antenna parameters and to provide solutions that would be useful for computerized antenna design. This effort shall include but not be limited to the following tasks:

1. An investigation of various mathematical modeling techniques for describing the radiation characteristics of antennas on the fuselage and/or wings of vehicles capable of reentry missions from space stations using:

a) wire-grid models
b) reaction concept
c) other types of models.

2. An investigation of the optimum numerical parameters and techniques for computational speed, storage, and accuracy such as:

a) location of test sources
b) testing functions
c) expansion modes.

3. A test of the validity and degree of accuracy of the various techniques by applying them to two-dimensional problems:

a) an infinite slot on infinite cylinders for the TE and TM cases (cylinders with square, elliptic, etc., cross-sections).

4. An investigation of low frequency techniques for the solution of various three-dimensional conducting bodies such as:

a) a finite slot on an infinite cylinder (wing)
b) a single slot on a spherical, spheroidial, ellipsoidial surfaces (fuselage)
c) coupled slots on the surfaces described in a) and b).

REFERENCES

1. J.H. Richmond, "TE-Wave Scattering by a Dielectric Cylinder of Arbitrary Cross-Section Shape," IEEE Trans., Vol. AP-14, July 1966.

2. J.H. Richmond, "Scattering by an Arbitrary Array of Parallel Wires," IEEE Trans., Vol. MTT-13, July 1965.

3. J.H. Richmond, "A Wire-Grid Model for Scattering by Conducting Bodies," IEEE Trans., Vol. AP-14, November 1966.

4. M. Traviezo-Diaz, G.A. Thiele, and H. Jones, "Radiation of a Monopole Antenna on the Base of a Conical Structure," ESL Technical Report 2622-2, 6 May 1969.

5. L.L. Tsai, "Analysis and Measurement of a Dipole Antenna Mounted Symmetrically on a Conducting Sphere or Cylinder," ESL Report 2648-3, July 1970.

6. "High Frequency Aircraft Antennas," ESL Final Technical Report 2235-5, 3 May 1968.

7. J.H. Richmond, "Theoretical Study of V Antenna Characteristics for the ATS-E Radio Astronomy Experiment," ESL Final Report 2619-1, 13 February 1969.

8. J.H. Richmond, "Computer Analysis of Three-Dimensional Wire Antennas," ESL Technical Report 2708-4, 22 December 1969.

9. G.A. Richards, "Reaction Formulation and Numerical Results for Multi-turn Loop Antennas and Arrays," Doctoral Dissertation, The Ohio State University, June 1970.

10. J. Richmond, L. Schwab, and R. Wickliff, "Scattering Characteristics of Some Thin Wire Chaff Elements," Technical Report 2584-8, 19 February 1970.

11. J. Freeland, Doctoral Dissertation, The Ohio State University (in preparation).

12. P.K. Agrawal, "Analysis of Coplanar TEM-Line Antenna Using Reaction Theorem," Thesis, The Ohio State University, 1969.

13. A.G. Jennetti, "Increased-Directivity Antennas," Doctoral Dissertation, The Ohio State University, March 1970.

14. R.L. Riegler, "Adaptive Optimization of Signal to Noise Ratio in Receiving Array," ESL Technical Report 2902-1, July 1970. Doctoral Dissertation, The Ohio State University, 1970.

APPENDIX I
DYADIC DIFFRACTION COEFFICIENT OF A STRAIGHT EDGE WITH NORMAL INCIDENCE

The diffraction of a scalar plane wave field by a half-plane has been solved exactly by Sommerfeld (Ref. BB-1). Pathak and Kouyoumjian (Ref. BB-2) have recently obtained an asymptotic solution for the spherical illumination of the edge. In this appendix, the results for the half-plane diffraction with normal incidence will be considered in the text to follow.

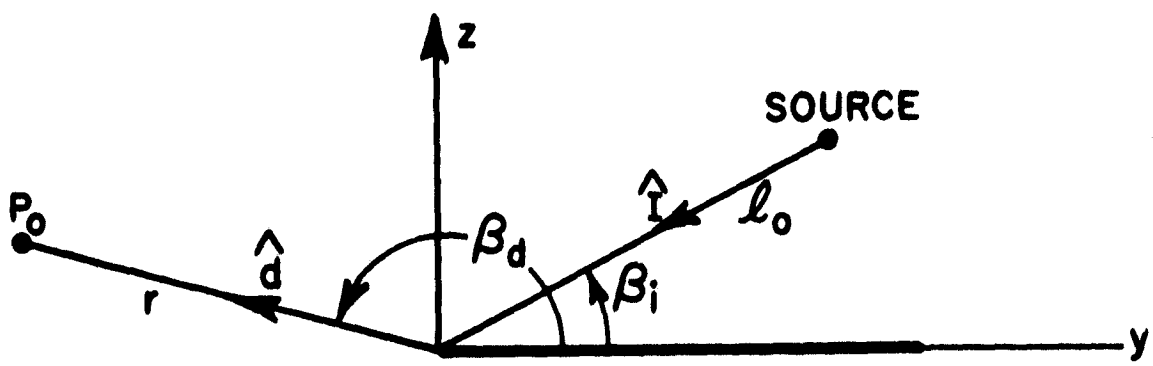

Let the total scalar field in space be denoted by U, then the total scalar field is the sum of a geometrical optics field and a diffracted field U^d. The soft boundary condition implies that U=0 at the surface of the half-plane; the hard boundary condition is $\partial U/\partial z = 0$. Let $U^i(\ell_o,\beta_i)$ be the field of the spherical wave incident at the edge of the half-plane. The diffracted fields for the soft and hard boundary conditions are

$$(BB\text{-}1) \qquad U^d_{\substack{s\\h}}(r,\beta_d) = U^i(\ell_o,\beta_i)\, D_{\substack{s\\h}}(\beta_d,\beta_i)\sqrt{\frac{\ell_o}{r(r+\ell_o)}}\; e^{-jkr}$$

where $D_s(\beta_d,\beta_i)$ and $D_h(\beta_d,\beta_i)$ are scalar diffraction coefficients for the soft and hard boundary conditions, respectively. They are given as

$$(BB\text{-}2) \qquad D_{\substack{s\\h}}(\beta_d,\beta_i) = -\frac{e^{-j\frac{\pi}{4}}}{2\sqrt{2\pi k}}\left[\frac{F(kLa_-)}{\cos\frac{\beta_d-\beta_i}{2}} \mp \frac{F(kLa_+)}{\cos\frac{\beta_d+\beta_i}{2}}\right]$$

where

$$(BB\text{-}3) \qquad F(kLa_{\mp}) = j2\sqrt{kLa_{\mp}}\, e^{jkLa_{\mp}} \cdot \int_{\sqrt{kLa_{\mp}}}^{\infty} e^{-j\tau^2} d\tau$$

$$(BB\text{-}4) \qquad a_{\mp} = 1 + \cos(\beta_d \mp \beta_i)$$

$$(BB\text{-}5) \qquad L = \frac{r\ell_o}{r+\ell_o}$$

In Eq. (BB-2), it shows that the diffraction coefficient is a function of β_d and β_i only. It is noted that $F(kLa_{\mp})$ is a correction factor need only in the transition regions of the reflection and shadow boundaries. Away from these boundaries, more precisely, when $kLa_{\mp} > 10$, $F(kLa_{\mp}) \simeq 1$ and it may be replaced by unity in Eq. (BB-2).

The integral in the $F(kLa_{\mp})$ factor is related to the Fresnel integral. It is given as

$$(BB\text{-}6) \qquad \int_X^{\infty} e^{-j\tau^2} d\tau = \int_0^{\infty} e^{-j\tau^2} d\tau - \int_0^X e^{-j\tau^2} d\tau$$

$$= \sqrt{\frac{\pi}{2}} \left\{ \left[\frac{1}{2} - C\left(\sqrt{\frac{\pi}{2}}\, x \right) \right] - j \left[\frac{1}{2} - S\left(\sqrt{\frac{\pi}{2}}\, x \right) \right] \right\}$$

The dyadic diffraction coefficient $\overline{\overline{D}}$ for the straight edge can be expressed in terms of the two scalar diffraction coefficients D_s and D_h for the soft and hard boundary conditions, respectively. For rays normally incident on the edge of a perfectly-conducting half-plane, the dyadic diffraction coefficient (Ref. BB-3) becomes

$$(BB\text{-}7) \qquad \overline{\overline{D}} = \hat{e}\hat{e}\, D_s + \hat{q}\hat{p}\, D_h$$

where

$\hat{e}$ is the unit vector tangent to the edge,

$\hat{p} = \hat{e} \times \hat{I}$ with $\hat{I}$ being the unit vector in the direction of the incident ray,

$\hat{q} = \hat{e} \times \hat{d}$ with $\hat{d}$ being the unit vector in the direction of the diffracted ray.

The vector diffracted electric field at P_o is

$$\text{(BB-8)} \qquad \overline{E}^d(r,\beta_d) = \overline{D}(\beta_d,\beta_i) \cdot \overline{E}^i(\ell_o,\beta_i)\sqrt{\frac{\ell_o}{r(r+\ell_o)}}\, e^{-jkr}$$

APPENDIX II

Employing differential geometry, Kouyoumjian (Ref. BB-4) has obtained the caustic distance ρ from the caustic to the point of diffraction on a curved edge to be

$$\text{(BB-10)} \qquad \frac{1}{\rho} = \frac{1}{\ell} - \frac{\hat{n}_e \cdot (\hat{I} - \hat{d})}{\rho_e \sin^2 \beta}$$

for spherical wave illumination of the edge. The parameters in Eq. (BB-10) are defined as follows:

ℓ is the distance from the phase center of the source to point of diffraction,

ρ_e is the radius of curvature of the edge,

$\hat{e}, \hat{n}_e$ are the unit vectors tangent and normal to the edge directed outward from the center of curvature,

$\hat{I}, \hat{d}$ are the unit vectors in the direction of the incident and diffracted rays at point of diffraction,

β is the angle between $\hat{e}$ and $\hat{I}$.

For a parabolic reflector antenna with a focal feed, it is found

$\rho_e = a$, the radius of the aperture

$\beta = \frac{\pi}{2}$, normal incidence

$\ell = \ell_o$, a fixed distance depending on the size of the parabolic reflector and its focal length f

for all points on the circular edge.

Substituting the above parameters into Eq. (BB-10), it becomes

$$\frac{1}{\rho_i} = \frac{1}{\ell_o} - \frac{\hat{n}_{ei} \cdot (\hat{I}_i - \hat{d}_i)}{a}$$

with i = 1,2 corresponding to the points of diffraction, Q_1 and Q_2, respectively, on the edge.

(a) Diffraction at Point Q_1 on the edge:

Referring to Fig. B-10, the unit vectors at Q_1 are found to be

$$\hat{n}_{e1} = \hat{x}' \cos\delta + \hat{y}' \sin\delta$$

$$\hat{e}_1 = \hat{x}' (-\sin\delta) + y' \cos\delta$$

$$\hat{I}_1 = \hat{x}' \sin\Psi_o \cos\delta + \hat{y}' \sin\Psi_o \sin\delta + \hat{z}' (-\cos\Psi_o)$$

$$\hat{d}_1 = \hat{x}' \frac{(v \sin\xi - a)\cos\delta}{r_1} + \hat{y}' \frac{(v \sin\xi - a)\sin\delta}{r_1} + \hat{z}' \frac{(v \cos\xi - z_o)}{r_1}$$

where $r_1 = \sqrt{(v \sin\xi - a)^2 + (v \cos\xi - z_o)^2}$

hence

$$\hat{n}_{e1} \cdot (\hat{I}_1 - \hat{d}_1) = \sin\Psi_o - \frac{(v \sin\xi - a)}{r_1}$$

Thus

$$\frac{1}{\rho_1} = \frac{1}{\ell_o} - \frac{1}{a}\left[\sin\Psi_o - \frac{(v \sin\xi - a)}{r_1}\right]$$

It is noted that $\sin\Psi_o = a/\ell_o$. Finally, the caustic distance ρ_1 becomes

$$\rho_1 = \frac{a\, r_1}{v \sin\xi - a} \qquad \text{(BB-11)}$$

(b) Diffraction at Point Q_2 on the Edge:

The unit vectors at Q_2 are found to be

$$\hat{n}_{e2} = \hat{x}' (-\cos\delta) + \hat{y}' (-\sin\delta)$$

$$\hat{e}_2 = \hat{x}' \sin\delta + \hat{y}' (-\cos\delta)$$

$$\hat{I}_2 = \hat{x}'(-\sin\Psi_o \cos\delta) + \hat{y}' (-\sin\Psi_o \sin\delta) + \hat{z}'(-\cos\Psi_o)$$

$$\hat{d}_2 = \hat{x}' \frac{(v \sin\xi + a)\cos\xi}{r_2} + \hat{y}' \frac{(v \sin\xi + a)\cos\delta}{r_2} + \hat{z}' \frac{(v \cos\xi - z_o)}{r_2}$$

where

$$r_2 = \sqrt{(v \sin \xi + a)^2 + (v \cos \xi - z_o)^2}.$$

It is fc th:

$$\hat{e}_2 \cdot (\hat{I}_2 - \hat{d}_2) = \sin \psi_o + \frac{v \sin \xi + a}{r_1}$$

Thus

$$\text{(BB-12)} \quad \frac{1}{\rho_2} = \frac{1}{\ell_o} - \frac{1}{a}\left[\sin \psi_o + \frac{(v \sin \xi + a)}{r_2}\right]$$

$$\rho_2 = -\frac{a\, r_2}{v \sin \xi + a}$$

REFERENCES

BB-1. Sommerfeld, A., Optics, New York: Academic Press, pp. 247-272, 1964.

BB-2. Pathak, P.H. and Kouyoumjian, R.G., "The Dyadic Diffraction Coefficient for a Perfectly-Conducting Wedge," Report 2183-4, 5 June 1970, ElectroScience Laboratory, Department of Electrical Engineering, The Ohio State University; prepared under Contract AF 19(628)-5929 for Electronic Systems Division, Air Force Systems Command.

BB-3. See Ref. (B-10).

BB-4. Kouyoumjian, R.G., "A Note on the Caustic Associated with Edge Diffraction," to be submitted for publication.